

Detailed Chemical Abundances in NGC 5824: Another Metal-Poor Globular Cluster with Internal Heavy Element Abundance Variations^{*}

Ian U. Roederer^{1,3†}, Mario Mateo¹, John I. Bailey III¹, Meghin Spencer¹,
Jeffrey D. Crane², Stephen A. Sackett²

¹*Department of Astronomy, University of Michigan, 1085 S. University Avenue, Ann Arbor, MI 48109, USA*

²*Carnegie Observatories, 813 Santa Barbara Street, Pasadena, CA 91101, USA*

³*Joint Institute for Nuclear Astrophysics and Center for the Evolution of the Elements, USA*

6 March 2022

ABSTRACT

We present radial velocities, stellar parameters, and detailed abundances of 39 elements derived from high-resolution spectroscopic observations of red giant stars in the luminous, metal-poor globular cluster NGC 5824. We observe 26 stars in NGC 5824 using the Michigan/Magellan Fiber System (M2FS) and two stars using the Magellan Inamori Kyocera Echelle (MIKE) spectrograph. We derive a mean metallicity of $[\text{Fe}/\text{H}] = -1.94 \pm 0.02$ (statistical) ± 0.10 (systematic). The metallicity dispersion of this sample of stars, 0.08 dex, is in agreement with previous work and does not exceed the expected observational errors. Previous work suggested an internal metallicity spread only when fainter samples of stars were considered, so we cannot exclude the possibility of an intrinsic metallicity dispersion in NGC 5824. The M2FS spectra reveal a large internal dispersion in $[\text{Mg}/\text{Fe}]$, 0.28 dex, which is found in a few other luminous, metal-poor clusters. $[\text{Mg}/\text{Fe}]$ is correlated with $[\text{O}/\text{Fe}]$ and anti-correlated with $[\text{Na}/\text{Fe}]$ and $[\text{Al}/\text{Fe}]$. There is no evidence for internal dispersion among the other α - or Fe-group abundance ratios. Twenty-five of the 26 stars exhibit a n -capture enrichment pattern dominated by r -process nucleosynthesis ($\langle [\text{Eu}/\text{Fe}] \rangle = +0.11 \pm 0.12$; $\langle [\text{Ba}/\text{Eu}] \rangle = -0.66 \pm 0.05$). Only one star shows evidence of substantial s -process enhancement ($[\text{Ba}/\text{Fe}] = +0.56 \pm 0.12$; $[\text{Ba}/\text{Eu}] = +0.38 \pm 0.14$), but this star does not exhibit other characteristics associated with s -process enhancement via mass-transfer from a binary companion. The Pb and other heavy elements produced by the s -process suggest a timescale of no more than a few hundred Myr for star formation and chemical enrichment, like the complex globular clusters M2, M22, and NGC 5286.

Key words: globular clusters: individual (NGC 5824) – nuclear reactions, nucleosynthesis, abundances – stars: abundances

1 INTRODUCTION

The number of globular clusters with spectroscopically-confirmed metallicity dispersions has grown dramatically over the last decade. These are generally among the most massive clusters, and many are also metal-poor. This list includes ω Cen (e.g., Norris & Da Costa 1995; Smith et al. 2000; Johnson & Pilachowski 2010;

Marino et al. 2011), M2 (Yong et al. 2014b), M19 (Johnson et al. 2015b), M22 (e.g., Da Costa et al. 2009; Marino et al. 2009), M54 (Carretta et al. 2010b), NGC 1851 (Yong & Grundahl 2008; Carretta et al. 2010c, 2011), NGC 3201 (Gonzalez & Wallerstein 1998; Simmerer et al. 2013), NGC 5286 (Marino et al. 2015), and Ter 5 (Origlia et al. 2011, 2013; Massari et al. 2014). Many of these clusters exhibit multiple sequences on the sub-giant branch on the color-magnitude diagram when using broadband optical photometry (e.g., Piotto et al. 2012), but NGC 3201 does not. To this list we add M92, where a high-precision differential analysis by Langer et al. (1998)

^{*} This paper includes data gathered with the 6.5 meter Magellan Telescopes located at Las Campanas Observatory, Chile.

[†] E-mail: iur@umich.edu

revealed one star with a metallicity significantly higher than other cluster members. Clusters that are not traditionally thought to contain internal metallicity spreads may exhibit small variations (< 0.03 dex) in Fe and other elements when pushed to the limit of high-precision abundance techniques, as in the case of NGC 6752 (Yong et al. 2013).

The metallicity dispersions in M22 and NGC 3201 have recently been called into question by Mucciarelli et al. (2015b,c). These authors report that the small dispersions observed could be artifacts of the analysis, and they have shown that spectroscopic gravities and Fe I lines may yield spurious metallicity results. Other contradicting results exist, too. Cohen et al. (2010) reported a spread in $[\text{Ca}/\text{H}]$ in NGC 2419 based on the Ca II near-infrared triplet. Mucciarelli et al. (2012) argued that this spread was caused by changes in the continuous opacity induced by severe Mg depletions in some stars, rather than a dispersion in Ca abundances. Intrinsic abundance dispersions based on the Ca II triplet have also been found in M22 by Da Costa et al. (2009). Mucciarelli et al. (2015c) reported that no metallicity dispersion exists in M22, but that result does not have a physical explanation since Mg shows no depletions in M22. While ongoing work seeks to re-examine the small metallicity dispersions (~ 0.1 dex) in some clusters, the range of metallicities is so large (~ 1 dex) in others that a legitimate cosmic dispersion must exist.

Some of these clusters, and others, are embedded in stellar halos extending beyond their tidal radii (Olszewski et al. 2009; Correnti et al. 2011; Kunder et al. 2014; Marino et al. 2014; Navin, Martell, & Zucker 2015). The most striking example is M54, which sits in the nucleus of the Sagittarius dwarf galaxy (e.g., Ibata, Gilmore, & Irwin 1995; Bellazzini et al. 2008). The others could be the tidally-stripped nuclei of former dwarf galaxies, suggesting formation within individual dark matter halos. It is important to establish which and how many clusters belong to this class of complex objects. This influences our understanding of their formation and evolution, and growing the membership of this class alleviates—slightly—the tension between cosmological simulations and the number of observed Milky Way satellites, also known as the “missing satellites” problem.

The elements heavier than the Fe group, hereafter known as n -capture elements, provide another perspective into the complex formation histories of globular clusters. In metal-poor clusters with no metallicity dispersion, the n -capture elements appear to have been produced predominantly, if not exclusively, by some form of rapid n -capture process (r -process; e.g., Gratton, Sneden, & Carretta 2004; Roederer et al. 2010b). This indicates a rapid enrichment timescale from core-collapse supernovae or neutron-star mergers. In the class of complex clusters, the n -capture elements show star-to-star variations in all cases where they have been studied (ω Cen, M2, M19, M22, NGC 1851, and NGC 5286). The heavy elements in these clusters were produced by each of the slow n -capture process (s -process) and the r -process, and often the proportions of r - and s -process material vary within each cluster. The r -process material is thought to have been present in the gas from which all stars formed. The s -process material is thought to have been produced in other stars within the cluster, ejected into the cluster ISM, and incorporated into the stars observed today (e.g., Smith et al. 2000). However, the chemical enrichment

scenarios to explain these signatures are neither simple nor uniform from one cluster to another.

Recent observations by Saviane et al. (2012) and Da Costa et al. (2014) revealed that NGC 5824 may also be a member of the class of complex globular clusters, similar to M2, M22, or NGC 5286. This southern cluster ($\alpha = 15:03:58.6$, $\delta = -33:04:05.6$) is the 14th most-luminous cluster around the Milky Way ($M_V = -8.85$; Harris 1996, 2010 edition), with a stellar mass of $\sim 6 \times 10^5 M_\odot$ (McLaughlin & van der Marel 2005). NGC 5824 is an outer halo cluster located 32.1 kpc from the Sun and 25.9 kpc from the Galactic center. There is moderate reddening along the line of sight, $E(B - V) = 0.14$, and NGC 5824 lies west of the Galactic bulge ($\ell = 332.6^\circ$) and north of the Galactic plane ($b = +22.1^\circ$). NGC 5824 does not show any split or broadened sequences in broadband optical color-magnitude diagrams (Piotto et al. 2002), but its blue horizontal branch is well-populated. Grillmair et al. (1995) identified light beyond the tidal radius of NGC 5824, but Carballo-Bello et al. (2014) did not detect any photometric signatures of an extended stellar halo around NGC 5824. Low-resolution spectroscopy of the Ca II triplet obtained by Da Costa et al. revealed a possible metallicity spread at the ≈ 0.1 dex level. No high-resolution spectra have been collected previously to examine the detailed kinematics and chemistry of this interesting cluster.

We present new high-resolution and high signal-to-noise (S/N) spectroscopy of red giants in NGC 5824. Our goals are (1) to confirm or refute the existence of a metallicity dispersion in NGC 5824; (2) to establish whether NGC 5824 exhibits the light-element abundance variations among O, Na, Mg, and Al that are common to globular clusters; and (3) to characterize the chemical (in)homogeneities of other α -elements, Fe-group elements, and n -capture elements. We describe our observations in Section 2, the radial velocity measurements in Section 3, the equivalent width (EW) measurements and line list in Sections 4 and 5, and the details of the abundance analysis in Sections 6 and 7. We present our abundance results in Section 8, weigh the evidence for a metallicity spread in Section 9, and discuss all other elements in Section 10. We summarize our conclusions in Section 11.

2 OBSERVATIONS

Our first set of observations were made using the Michigan/Magellan Fiber System (M2FS) and MSpec double spectrograph (Mateo et al. 2012; Bailey et al. 2012) mounted on the Nasmyth platform at the 6.5 m Landon Clay Telescope (Magellan II) at Las Campanas Observatory, Chile. M2FS uses fiber plug plates to achieve high multiplexing capability over a 30'-diameter field of view. We observed 50 candidate members of NGC 5824 and 11 blank sky positions. Three observations were made on 2015 April 15, 2015 April 19, and 2015 April 20, with a total integration time of 11.5 h.

Our observations were made in HiRes mode with $95 \mu\text{m}$ entrance slits. This setup delivers spectral resolving power $R \equiv \lambda/\Delta\lambda \sim 34,000$, as measured from isolated Th or Ar emission lines in the comparison lamp spectra. This corresponds to ≈ 6.3 pixels per resolution element (RE). The

Table 1. Magnitudes, S/N Estimates, Velocities, and Model Atmosphere Parameters for Stars Observed in NGC 5824

Star	V	S/N pix ⁻¹ (4570 Å)	V_r (km s ⁻¹)	T_{eff} (K)	log g	v_t (km s ⁻¹)	[M/H]
11001198	16.35	51	-24.5 (0.6)	4261	1.01	2.20	-2.08
12001300	16.24	40	-28.0 (0.6)	4337	1.02	1.85	-1.96
21000267	15.61	62	-28.7 (0.4)	4075	0.55	2.00	-1.92
21000688	15.75	47	-42.5 (0.6)	4083	0.62	2.20	-1.95
21002944	15.39	54	-25.8 (0.4)
31003079	16.80	20	-26.2 (0.7)
32004229	16.52	27	-29.6 (1.1)
32004840	16.69	27	-26.4 (1.2)
41000940	16.47	40	-26.7 (0.6)	4345	1.12	1.65	-1.87
41001607	16.15	50	-32.9 (0.8)	4235	0.91	2.35	-1.96
41002449	17.07	28	-20.8 (0.9)
41003361	17.06	29	-25.1 (0.8)
42006307	16.34	46	-23.5 (0.8)	4328	1.06	1.55	-1.93
42006712	17.27	25	-36.5 ^a
42007331	16.82	28	-18.0 (0.7)
42007539	15.95	36	-27.8 (0.8)	4188	0.79	1.90	-1.90
42007983	17.09	18	-29.6 ^a
42008343	16.49	41	-22.0 (0.6)	4392	1.16	1.55	-1.98
42008555	16.98	40	-27.2 (0.9)	4488	1.42	1.45	-1.88
42009955	15.92	53	-23.0 (0.8)	4200	0.79	2.20	-1.93
42010124	15.88	52	-34.3 (0.9)	4146	0.73	2.10	-1.92
42010715	16.62	38	-29.6 (0.7)	4378	1.20	1.90	-2.00
42011097	16.65	45	-24.7 (0.8)	4383	1.22	1.75	-1.93
42011404	15.97	34	-28.1 (1.1)	4190	0.80	1.95	-1.82
42011439	16.90	34	-20.8 (0.5)
42011588	16.42	31	-33.9 (0.7)
42012172	16.96	27	-28.7 (0.8)
42012437	17.06	34	-23.0 (0.6)
42012704	16.19	51	-29.7 (0.7)	4248	0.94	2.20	-1.99
42013014	16.24	43	-26.9 (0.6)	4211	0.93	2.30	-1.89
51000173	16.89	27	-23.6 (0.4)
52005710	16.96	30	-34.8 (0.6)	4453	1.39	1.40	-1.90
52009395	17.37	29	-25.5 (0.8)
61000086	16.96	27	-28.7 (0.7)
61000142	17.04	31	-29.0 (1.1)
61000144	16.40	33	-34.3 (1.0)	4293	1.06	1.85	-1.90
61000182	16.98	31	-25.0 (0.4)
61000397	16.31	39	-23.9 (0.9)	4242	0.98	2.10	-1.97
61000826	16.27	43	-34.8 (0.7)	4312	1.02	1.65	-2.01
61001052	16.79	29	-25.9 (0.8)
61001690	17.11	27	-21.6 (0.8)
61001836	16.88	36	-24.1 (0.8)
61003283	16.28	36	-28.6 (0.4)
61005163	15.91	52	-21.1 (0.5)	4198	0.78	2.10	-1.85
61007408	16.17	51	-34.6 (0.9)	4220	0.91	1.80	-2.04
61007565	15.96	58	-28.0 (0.8)	4159	0.77	1.85	-1.78
61008247	16.43	42	-34.4 (0.9)	4360	1.12	2.00	-2.10
62000027	16.43	33	-27.7 (0.9)
71000779	17.03	25	-20.1 (1.0)
71002877	15.81	55	-27.3 (0.8)	4110	0.67	2.15	-1.72

^a Velocity derived from a single, noisy measurement only; uncertainty is likely to be 1.5 km s⁻¹ or greater.

spectral resolution varies by ≈ 7 per cent from one fiber tetrises to another due to the alignment of the fiber tetrises with the slits. We use a custom set of order-isolation filters to observe orders 77–80, which covers roughly $4425 \leq \lambda \leq 4635$ Å for each target. Figure 1 illustrates the entire M2FS spectrum of one star in our sample, 21000267.

Targets were chosen from the list of probable members given by Da Costa et al. (2014). Stars observed with M2FS

are on the upper red giant branch (RGB) in NGC 5824 and are ≈ 1 to 3 magnitudes brighter than the horizontal branch. Some data reduction (merging data from different CCD chip amplifiers, stacking images, masking cosmic rays, and subtracting scattered light) was performed using PYTHON routines written by J. I. B. Standard IRAF routines were used to perform all other tasks (flatfielding, extraction, wavelength calibration, spectra co-addition, ve-

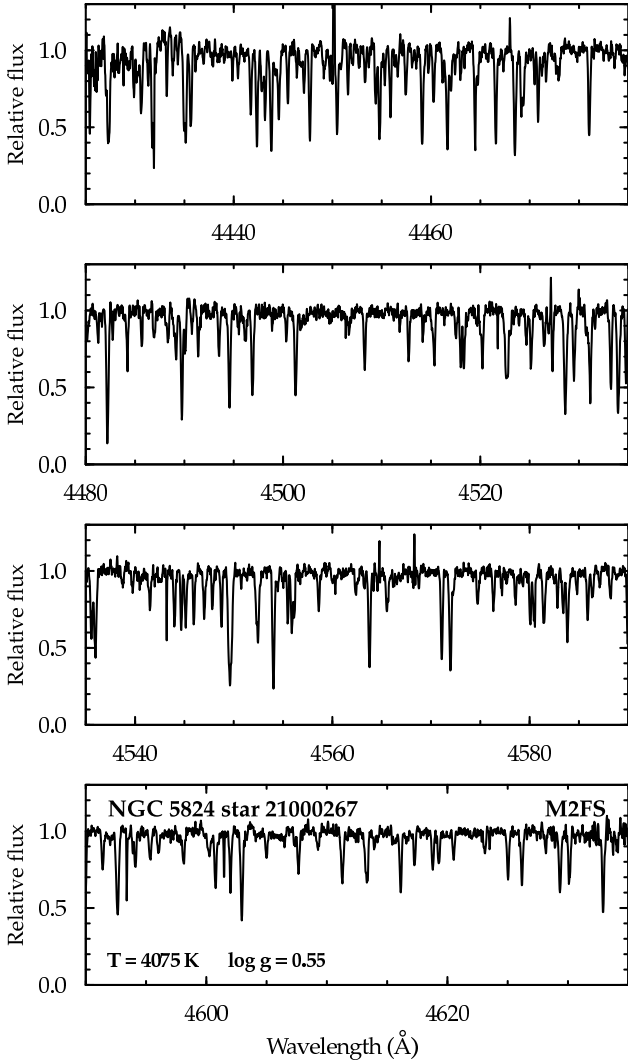


Figure 1. The M2FS spectrum of star 21000267.

locity shifting, and continuum normalization). The M2FS observations of NGC 5824 were made during dark time. Sky contamination was found to be negligible, so no sky subtraction was performed. Table 1 lists the V magnitudes (from Da Costa et al.) and S/N ratios per pixel in the co-added M2FS spectra. Our proposed M2FS integration times were shortened considerably due to poor weather during the M2FS block run in April, 2015. We measure radial velocities for all targets observed (Section 3), but a reliable chemical analysis (Section 7) is only possible for the brightest targets.

After an initial analysis of the M2FS spectra, two stars with nearly identical stellar parameters but differing levels of n -capture elements were selected for additional observations. Stars 42009955 and 61005163 were observed on 2015 June 16 using the Magellan Inamori Kyocera Echelle (MIKE) spectrograph (Bernstein et al. 2003), which is also mounted on the Nasmyth platform at Magellan II (but not simultaneously with M2FS). These spectra were taken with the $0''.7 \times 5''.0$ slit, yielding a resolving power of $R \sim 41,500$ in the blue and $R \sim 34,700$ in the red as measured from isolated Th and Ar emission lines in the comparison lamp images. This corresponds to ≈ 2.5 and 2.1 pixels RE^{-1} on

the blue and red arms, respectively. The blue and red arms are split by a dichroic at ≈ 4950 Å. This setup achieves complete wavelength coverage from 3350–9150 Å, although only the spectra longward of ≈ 3800 Å have signal sufficient to perform a detailed abundance analysis. Data reduction, extraction, sky subtraction, and wavelength calibration were performed using the CARPY MIKE data reduction pipeline (see, e.g., Kelson 2003). Coaddition and continuum normalization were performed within IRAF. The total integration times were 4.2 h and 3.3 h for stars 42009955 and 61005163, respectively. The S/N ratios of the co-added MIKE spectra range from $\approx 25/1$ near 3950 Å to $\approx 140/1$ near 6750 Å.

2.1 Comparing the M2FS and MIKE Spectra

Figure 2 illustrates a portion of the region of overlap between the M2FS and MIKE spectra for one of the stars in common, 61005163. The differences, resampled to the M2FS pixel spacing, are shown in the bottom of each panel in Figure 2. Qualitatively, the agreement between the spectra appears excellent, and we now attempt to quantify the degree of similarity.

Figure 3 shows a histogram of the residuals of the normalized M2FS and MIKE spectra for each of the two stars. Only wavelengths from 4430 to 4630 Å are included. The mean difference is -0.096 per cent, which reflects the relative continuum normalization of the two spectra. The standard deviation of the residuals is 4.0 per cent. The S/N ratios of the M2FS spectra of these two stars are $\approx 52/1$ per 0.0292 Å pixel, and the S/N ratios of the MIKE spectra are $\approx 63/1$ per 0.044 Å pixel. After converting to a common pixel size, a residual of ≈ 2.7 per cent can be accounted for by photon noise alone. The differing resolution of the two instruments accounts for another ≈ 0.7 per cent of the residuals, if we assume that absorption lines account for ≈ 20 per cent of the spectrum. This leaves $(0.040^2 - 0.027^2 - 0.007^2)^{1/2} \approx 2.9$ per cent unaccounted for, which we assume includes errors in the flatfielding, cosmic ray removal, sky subtraction, order merging, etc. We conclude that the M2FS and MIKE spectra are identical to within a few per cent. In Sections 4 and 8.1, we compare EWs and abundances derived from the two sets of spectra.

3 RADIAL VELOCITY MEASUREMENTS

We measure radial velocities for each M2FS observation using the IRAF FXCOR task to cross-correlate, order-by-order, against a template. We use one high-S/N spectrum of 21000267 as the template. We establish the zeropoint of this spectrum by using SPLOT to measure the wavelengths of 51 Fe I lines; we then compare with the laboratory wavelengths presented by Nave et al. (1994). The velocity zeropoint of the template is accurate to better than 0.2 km s^{-1} . The statistical uncertainties associated with each cross-correlation relative to the template vary with S/N, ranging from 0.4 km s^{-1} for the brightest targets to 1.3 km s^{-1} for the faintest ones. We estimate these uncertainties based on repeat observations of each star. We estimate the absolute velocity uncertainty to be $\approx 0.2 \text{ km s}^{-1}$, based on observations of the metal-poor standard star HD 122563 taken with the same M2FS configuration in February, 2015.

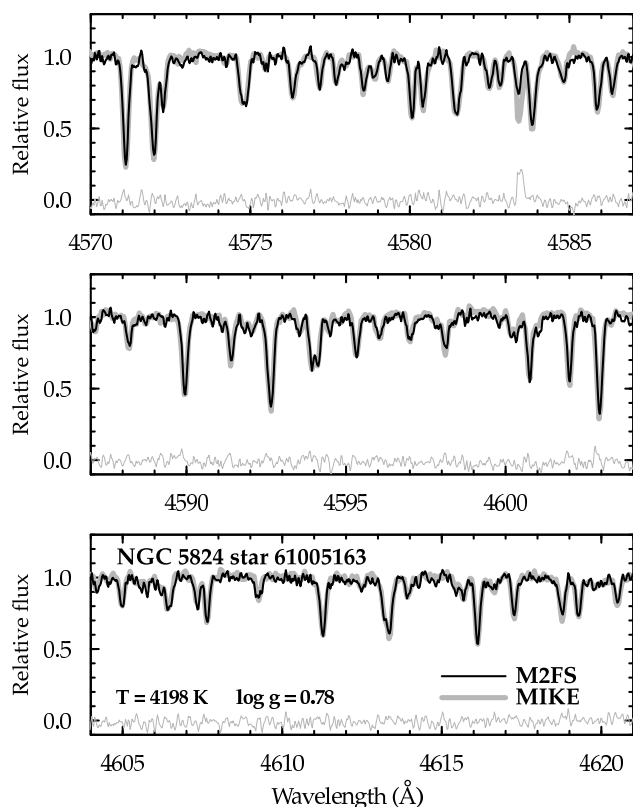


Figure 2. Portions of the M2FS and MIKE spectra of star 61005163. The M2FS spectrum is shown by the black line, and the MIKE spectrum is shown by the bold gray line. The thin gray line at the bottom of each panel shows the residual between the two spectra on the same scale.

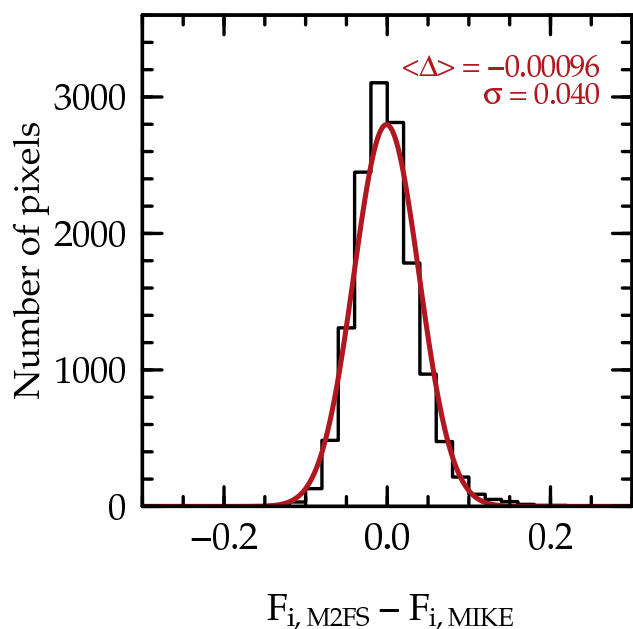


Figure 3. Residuals in the normalized flux between the M2FS and MIKE spectra of stars 42009955 and 61005163. The mean difference and standard deviation are printed and illustrated by the red curve.

Table 2. Equivalent Width Measurements for Lines Detected in the M2FS Spectra

Star	Species	λ (Å)	EW (mÅ)
11001198	Mg I	4571.10	142.5
11001198	Ca I	4526.94	36.2
11001198	Ca I	4578.55	39.1
11001198	Ti I	4453.70	29.7
11001198	Ti I	4481.26	43.7

The complete version of Table 2 is available in machine-readable format in the Supplementary Information found in the online edition of the journal. Only a small portion is shown here to illustrate its form and content.

Note— All abundances derived from lines with no EW reported in Table 2 have been derived by spectrum synthesis matching.

We report heliocentric radial velocities, V_r , for each star in Table 1. We calculate heliocentric corrections using the IRAF RVCORRECT task. The velocities in Table 1 represent a weighted mean of our three observations. The weights roughly correspond to the S/N obtained in each set of observations, with a weight of 1 for the first and third epochs and a weight of 3 for the second epoch. Our radial velocities differ by only $1.9 \pm 0.2 \text{ km s}^{-1}$ ($\sigma = 9.1 \text{ km s}^{-1}$) from those reported by Da Costa et al. (2014).

The mean systemic radial velocity for NGC 5824, based on 50 stars, is $-27.4 \pm 0.7 \text{ km s}^{-1}$ ($\sigma = 4.9 \text{ km s}^{-1}$). This agrees with the values measured by Da Costa et al. (2014), $-28.9 \pm 1.0 \text{ km s}^{-1}$, and Dubath et al. (1997), $-26.0 \pm 1.6 \text{ km s}^{-1}$. The dispersion of our velocity measurements, 4.9 km s^{-1} , is considerably smaller than the core velocity dispersion derived from the integrated-light spectra of Dubath et al., $11.1 \pm 1.6 \text{ km s}^{-1}$. This may be expected since our targets mostly sample the outer regions of the cluster ($0.9 < r_h < 14$, where $r_h = 0.45$ arcmin is the half-light radius given by Harris 1996).

We measure radial velocities from the MIKE spectra of stars 42009955 and 61005163 by cross-correlating a late-type metal-poor template against the echelle order containing the Mg I b lines, as described in Roederer et al. (2014a). The MIKE velocity zeropoint is reliable to $\approx 0.2 \text{ km s}^{-1}$ (e.g., Roederer & Kirby 2014). The heliocentric radial velocities measured from the MIKE spectra of stars 42009955 and 61005163, $-21.4 \pm 0.7 \text{ km s}^{-1}$ and $-20.8 \pm 0.7 \text{ km s}^{-1}$, are in agreement with those measured two months earlier using M2FS, $-23.0 \pm 0.8 \text{ km s}^{-1}$ and $-21.1 \pm 0.5 \text{ km s}^{-1}$. Our data offer no evidence for radial velocity variations for either star.

4 EQUIVALENT WIDTHS

We measure EWs from the spectra using a semi-automated routine, EW.PRO, that fits Voigt (or Gaussian) line profiles to continuum-normalized spectra. As discussed in Roederer et al. (2014a), all fits are presented to the user for approval, modification, or rejection. The EWs measured in the M2FS spectra are listed in Table 2, and the EWs measured in the MIKE spectra are listed in Table 3. The full list of lines examined in the M2FS spectra is shown in Table 4.

EWs measured from MIKE spectra are useful to demon-

Table 3. Equivalent Width Measurements for Lines Detected in the MIKE Spectra

Species	λ (Å)	E.P. (eV)	$\log gf$	Ref.	EW 42009955 (mÅ)	EW 61005163 (mÅ)
Li I	6707.80	0.00	0.17	1	limit	limit
O I	6300.30	0.00	−9.78	2	limit	...
O I	7771.94	9.14	0.37	2	limit	6.2
O I	7774.17	9.14	0.22	2	limit	8.0
O I	7775.39	9.14	0.00	2	limit	7.1

The complete version of Table 3 is available in machine-readable format in the Supplementary Information found in the online edition of the journal. Only a small portion is shown here to illustrate its form and content.

Notes— Lines denoted “limit” were not detected, and upper limits have been derived. Lines denoted “synth” yielded abundances via spectrum synthesis matching.

References— (1) Smith, Lambert, & Nissen 1998; (2) NIST; (3) Aldenius, Lundberg, & Blackwell-Whitehead 2009; (4) Lawler & Dakin 1989, using HFS from Kurucz & Bell 1995; (5) Lawler et al. 2013; (6) Wood et al. 2013; (7) Lawler et al. 2014, using HFS from Kurucz & Bell 1995; (8) Wood et al. 2014b; (9) Sobek, Lawler, & Sneden 2007; (10) Nilsson et al. 2006; (11) Booth et al. 1984; (12) Den Hartog et al. 2011 for both $\log gf$ value and HFS; (13) Ruffoni et al. 2014; (14) NIST, using HFS from Kurucz & Bell 1995; (15) Wood et al. 2014a; (16) Roederer & Lawler 2012; (17) Biémont et al. 2011; (18) Ljung et al. 2006; (19) NIST, using HFS/IS from McWilliam 1998 when available; (20) Lawler, Bonvallet, & Sneden 2001, using HFS from Ivans et al. 2006; (21) This study; (22) Roederer, Marino, & Sneden 2011; (23) Lawler et al. 2009; (24) Li et al. 2007, using HFS from Sneden et al. 2009; (25) Ivarsson, Litzén, & Wahlgren 2001, using HFS from Sneden et al. 2009; (26) Den Hartog et al. 2003, using HFS/IS from Roederer et al. 2008 when available; (27) Lawler et al. 2006, using HFS/IS from Roederer et al. 2008 when available; (28) Lawler et al. 2001b, using HFS/IS from Ivans et al. 2006; (29) Roederer et al. 2012b; (30) Den Hartog et al. 2006; (31) Lawler et al. 2001a; (32) Wickliffe, Lawler, & Nave 2000; (33) Lawler et al. 2008; (34) Lawler et al. 2007; (35) Biémont et al. 2000, using HFS/IS from Roederer et al. 2012b; (36) Nilsson et al. 2002.

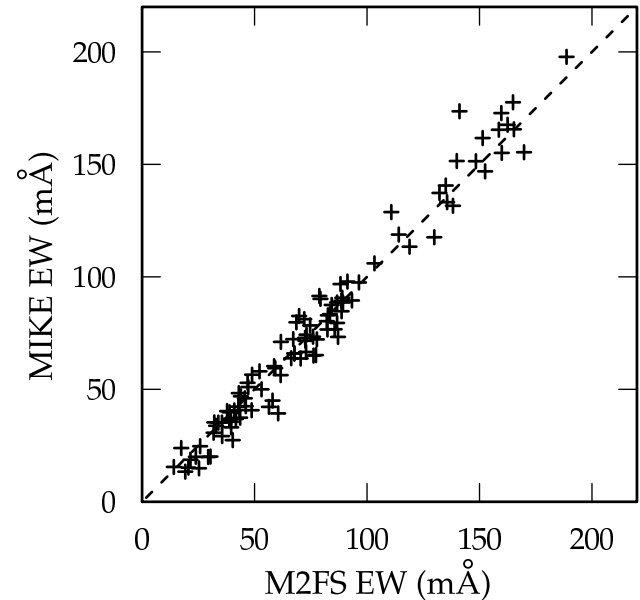
strate the integrity of EWs measured from M2FS spectra. Roederer et al. (2014a) found that EWs measured using EW.PRO were statistically identical among spectra obtained with three different spectrographs—MIKE, the Tull Coudé Spectrograph, and the High Resolution Spectrograph (HRS). (The Tull and HRS instruments are at McDonald Observatory, Texas). Bedell et al. (2014) performed an analysis of EWs measured from high-quality asteroid-reflected solar spectra taken with MIKE and ESPaDOnS. (ESPaDOnS is at the the Canada-France-Hawaii Telescope.) They found abundance differences at the ≈ 0.04 dex level. This comprised the largest component of the error budget in their differential analysis, but it is sufficiently small for our purposes. Figure 4 compares the EWs measured with MIKE and M2FS for 103 lines in common in the spectra of stars 42009955 and 61005163. We find a difference of 0.25 ± 0.78 mÅ ($\sigma = 7.9$ mÅ), which is not significant, indicating that the M2FS EWs are also consistent with external scales.

Table 4. List of Lines Examined in M2FS Spectra

Species	Wavelength (Å)	E.P. (eV)	$\log gf$	Ref.
Mg I	4571.10	0.00	−5.62	1
Ca I	4526.94	2.71	−0.42	1
Ca I	4578.55	2.52	−0.56	1
Sc II	4431.35	0.60	−1.97	2
Ti I	4449.14	1.89	+0.47	3

The complete version of Table 4 is available in machine-readable format in the Supplementary Information found in the online edition of the journal. Only a small portion is shown here to illustrate its form and content.

References— (1) NIST; (2) Lawler & Dakin 1989, using HFS from Kurucz & Bell 1995; (3) Lawler et al. 2013; (4) Wood et al. 2013; (5) Lawler et al. 2014, using HFS from Kurucz & Bell 1995; (6) Sobek, Lawler, & Sneden 2007; (7) Booth et al. 1984; (8) Ruffoni et al. 2014; (9) Wood et al. 2014a; (10) NIST, using HFS/IS from McWilliam 1998; (11) This work; (12) Lawler et al. 2009; (13) Den Hartog et al. 2003, using HFS/IS from Roederer et al. 2008 when available; (14) Lawler et al. 2006, using HFS/IS from Roederer et al. 2008 when available; (15) Lawler et al. 2001b, using HFS/IS from Ivans et al. 2006 when available; (16) Wickliffe, Lawler, & Nave 2000.

**Figure 4.** Comparison of EWs measured in M2FS and MIKE spectra of stars 42009955 and 61005163. The dashed line marks the one-to-one correspondence.

5 ATOMIC DATA

Tables 3 and 4 include references for the atomic data. We privilege $\log gf$ values from recent laboratory studies whenever possible, since these investigations frequently deliver ≈ 5 per cent precision (≈ 0.02 dex) or better. We also attempt to use a single source for the $\log gf$ values of a given species whenever possible, to minimize any systematic offsets from one study to another. Our goal in making these choices is to minimize the impact of systematics arising from the set of lines examined. As we show in Section 8.1, this goal can be achieved in most cases.

Table 5. List of Hyperfine Component Patterns for Heavy Elements Sorted by Species and Wavelength

Species	Isotope	Wavelength (Å)	E.P. (eV)	$\log gf^a$
Ba II	137	4553.9980	0.000	−0.6660
Ba II	137	4554.0000	0.000	−0.6660
Ba II	137	4554.0010	0.000	−1.0640
Ba II	135	4554.0020	0.000	−0.6660
Ba II	135	4554.0030	0.000	−0.6660

The complete version of Table 5 is available in machine-readable format in the Supplementary Information found in the online edition of the journal. Only a small portion is shown here to illustrate its form and content.

^a The $\log gf$ values of each isotope are normalized to the total $\log gf$ value for the transition.

Hyperfine splitting (HFS) structure and isotope shifts (IS) are included in the spectrum synthesis when these data are available. We adopt an isotopic ratio for $^{12}\text{C}/^{13}\text{C}$ of 4. For Cu, we adopt the solar isotopic ratio, $^{63}\text{Cu}/^{65}\text{Cu} = 2.24$. We adopt r -process isotopic fractions for Ba, Nd, Sm, Eu, and Pb using the values presented in Sneden, Cowan, & Gallino (2008). For star 61005163, we instead adopt an appropriate mixture of r - and s -process isotopic fractions (see Section 10.3). At the request of the referee, we have included the HFS and IS component patterns for lines of n -capture elements studied in this work. These are presented in Table 5. We emphasize that these data simply echo those given in the references to Table 3.

The La II line at 4522.37 Å was not covered by the laboratory study of Lawler, Bonvallet, & Sneden (2001), but it is the only reliable La II line that appears in our M2FS spectra. We use a high-resolution spectrum of the r -process-rich standard star BD+17 3248, a red giant with $[\text{Fe}/\text{H}] = -2.1$ (Cowan et al. 2002), to derive an empirical $\log gf$ value for this line. Our examination of five other La II lines in BD+17 3248 yields $\log gf = -1.22 \pm 0.10$ for the line at 4522.37 Å. No HFS data are available for this line. It falls on the linear part of the curve of growth in the spectra of NGC 5824 red giants and the spectrum of BD+17 3248, so errors resulting from the neglect of HFS in our spectrum synthesis should be minimal.

6 MODEL ATMOSPHERE PARAMETERS

We calculate effective temperatures, T_{eff} , using the dereddened $V - I$ color- T_{eff} relation from Alonso et al. (1999), assuming $E(B - V) = 0.14$ (Zinn 1980; Reed, Hesser, & Shawl 1988) and the Cardelli et al. (1989) extinction coefficients. We transform the Da Costa et al. (2014) $V - I$ colors, measured in the standard Johnson-Cousins system, to the Johnson system using the relation given by Bessell (1979). A second step is frequently employed by fitting a relationship between a magnitude (often K) and T_{eff} , which reduces the impact of photometric errors and differential reddening (e.g., Carretta et al. 2007; Roederer & Thompson 2015). This approach assumes that the RGB has no intrinsic spread at a given color. This as-

sumption may be invalid for NGC 5824 since an internal metallicity spread may be present, so we do not employ this second step when calculating T_{eff} . Monte Carlo error propagation calculations indicate that the statistical uncertainties on T_{eff} from all sources of error (intrinsic scatter in the color- T_{eff} relation, photometric error, and uncertainty in the reddening) are ≈ 145 K. The optional second step—fitting and interpolating a relationship between K and T_{eff} —yields statistical uncertainties ≈ 40 –50 K, which is considerably better. This demonstrates why the second step is preferable when applicable.

We calculate the log of the surface gravity, $\log g$, using the relation $\log g = 4 \log(T_{\text{eff},*}) + \log(M/M_{\odot}) - 0.4(M_{\text{bol},\odot} - M_{\text{bol},*}) - 10.61$. The constant 10.61 is derived from the solar values given in Cox (2000), the quantity $M_{\text{bol},*}$ is given by $BC_V + m_V - (m - M)$, and BC_V is given by eq. 18 of Alonso et al. (1999). We assume masses of $0.8 \pm 0.15 M_{\odot}$ for all stars. We adopt the distance modulus given by Harris (1996), $m - M = 17.94 \pm 0.05$, which is based on the magnitude of the horizontal branch measured by Brocato et al. (1996). Our Monte Carlo calculations indicate that statistical uncertainties in the $\log g$ values are ≈ 0.14 dex. This quantity is dominated by uncertainties in T_{eff} and mass estimates.

We interpolate model atmospheres from the ATLAS9 grid of α -enhanced models (Castelli & Kurucz 2003), using an interpolator provided by A. McWilliam (2009, private communication). We derive abundances using a recent version of the MOOG line analysis software (Sneden 1973), with updates described in Sobeck et al. (2011). We determine microturbulent velocities, v_t , by requiring no trend between the line strength, parameterized by $\log(\text{EW}/\lambda)$, and abundance derived from Fe I lines. We estimate a statistical uncertainty of $\approx 0.1 \text{ km s}^{-1}$ in v_t for a fixed set of T_{eff} and $\log g$. We set the model metallicity, $[\text{M}/\text{H}]$, equal to the Fe abundance derived from Fe II lines and adjust the microturbulent velocity and metallicity iteratively. We also iteratively cull Fe I and II lines giving abundances more than 2σ from the mean. We consider the model parameters to have converged when subsequent adjustment of v_t is less than 0.05 km s^{-1} , adjustment of the model $[\text{M}/\text{H}]$ is less than 0.03 dex, and all Fe I and II lines agree to within 2σ .

Systematic sources of uncertainty are undoubtedly larger than the statistical errors noted here, but they have little effect on the relative abundances of stars in the same evolutionary state. We discuss the impact of these uncertainties in Section 9.2.

The adopted model atmosphere parameters are listed in Table 1 for stars with moderate or high S/N levels and $T_{\text{eff}} > 4000$ K. We examine the detailed abundance patterns of these 26 stars. Star 21002944 also has superb S/N, but it may be on the AGB. Assuming a mass of $0.65 M_{\odot}$ (Gratton et al. 2010), we estimate a temperature of 3890 K, which is nearly 200 K cooler than the next-coolest giant. Our method may not be applicable to stars this cool without additional modification, and we aim to preserve a differential quality to the analysis. We do not analyze the abundances in star 21002944 and will not discuss it further.

7 ANALYSIS

Most abundances are derived using an adaptation of the batch mode capabilities of MOOG, forcing theoretical EWs to match the observed ones by adjusting the abundance. Other abundances are derived by matching synthetic to observed spectra. We adopt the latter method when lines are too blended to measure reliable EWs or when HFS or IS could affect the derived abundance. In a few cases, we report 3σ upper limits on the abundance using a version of the formula presented on p. 590 of Frebel et al. (2008), which is derived from equation A8 of Bohlin et al. (1983).

We assume local thermodynamic equilibrium (LTE) holds for the line-forming layers of the atmosphere for all species except Na I (Lind et al. 2011) and K I (Takeda et al. 2002). Both of these species—and O, discussed below—can only be detected in the MIKE spectra. The non-LTE corrections for the Na I lines at 5682, 5688, 6154, and 6160 Å range from -0.02 to -0.08 dex. Non-LTE corrections for the K I line at 7698 Å are ≈ -0.48 dex. We include an additional 0.1 dex statistical uncertainty in our error estimates to account for uncertainties in the corrections. Non-LTE corrections for each of the three high-excitation O I 7771, 7774, and 7775 Å triplet lines are expected to be substantial, but the stellar parameters of stars 42009955 and 61005163 are far from the edge of the grid of corrections presented by Fabbian et al. (2009), so we do not employ them. We caution that the LTE O abundances derived from these lines are likely overestimated, and we only recommend their use in a differential sense. The [O I] line at 6300 Å, which is expected to form under LTE, is weak and cannot be reliably measured even after removing the telluric lines.

No C or N lines are detected in our M2FS spectra. In the two MIKE spectra, C abundances are derived from the CH $A^2\Delta - X^2\Pi$ G band (≈ 4290 – 4330 Å) using a line list provided by B. Plez (2007, private communication). N abundances are derived from the CN $B^2\Sigma - X^2\Sigma$ violet band (≈ 3875 – 3885 Å) using the line list from Kurucz & Bell (1995) after setting the C abundance using the CH G band. We use the spectrum synthesis matching technique to derive the C and N abundances.

8 RESULTS

Table 6 lists the mean abundances derived for each element in each star observed with M2FS. Tables 7 and 8 list the mean abundances derived from the MIKE spectra of stars 42009955 and 61005163. The abundances in Tables 7 and 8 reflect the non-LTE corrections discussed in Section 7. We use standard definitions of elemental abundances and ratios in these tables. For element X, the logarithmic abundance is defined as the number of X atoms per 10^{12} hydrogen atoms, $\log \epsilon(X) \equiv \log_{10}(N_X/N_H) + 12.0$. For elements X and Y, $[X/Y]$ is the logarithmic abundance ratio relative to the solar ratio on the Asplund et al. (2009) abundance scale, defined as $\log_{10}(N_X/N_Y) - \log_{10}(N_X/N_Y)_\odot$, using like ionization states; i.e., neutrals with neutrals and ions with ions. Abundances or ratios denoted with the ionization state indicate the total elemental abundance as derived from transitions of that particular state.

Four sets of uncertainties are listed in these tables. The

Table 9. Mean Abundances in NGC 5824 Determined from M2FS Spectra

Ratio	Species	Mean	Std. err.	Std. dev.	N _{stars}
[Fe/H]	I	−2.38	0.02	0.08	25
[Fe/H]	II	−1.94	0.02	0.08	25
[Mg/Fe]	I	−0.20	0.06	0.28	25
[Ca/Fe]	I	+0.20	0.02	0.10	25
[Sc/Fe]	II	−0.02	0.04	0.15	15
[Ti/Fe]	I	−0.04	0.02	0.09	25
[Ti/Fe]	II	+0.29	0.02	0.08	25
[V/Fe]	I	−0.26	0.03	0.14	24
[Cr/Fe]	I	−0.25	0.02	0.08	25
[Cr/Fe]	II	+0.13	0.03	0.15	25
[Mn/Fe]	I	−0.38	0.06	0.16	7
[Ni/Fe]	I	−0.11	0.03	0.14	25
[Sr/Fe]	I	−0.36	0.04	0.17	22
[Ba/Fe]	II	−0.55	0.05	0.24	25
[La/Fe]	II	−0.14	0.03	0.11	12
[Ce/Fe]	II	−0.19	0.02	0.10	25
[Nd/Fe]	II	−0.04	0.03	0.15	25
[Sm/Fe]	II	+0.12	0.03	0.16	24
[Eu/Fe]	II	+0.11	0.02	0.12	25
[Dy/Fe]	II	+0.16	0.04	0.17	22

Note—Star 61005163 has been excluded from the data presented in this table.

statistical uncertainty, σ_{stat} , is given by equation A17 of McWilliam et al. (1995). This includes uncertainties in the EW, line profile fitting, $\log gf$ values, and non-LTE corrections, if any. The total uncertainty, σ_{tot} , is given by equation A16 of McWilliam et al. This includes the statistical uncertainty and reflects uncertainties in the model atmosphere parameters. The other two uncertainties, σ_{neut} and σ_{ions} , are useful when constructing abundance ratios among different elements. We recommend that σ_{neut} for element A be added in quadrature with σ_{stat} for element B when computing the ratio $[A/B]$ when B is derived from lines of the neutral species. Similarly, we recommend using σ_{ions} instead of σ_{neut} when element B is derived from lines of the ionized species. These latter two sets of uncertainties are omitted for the [Fe/H] ratios.

Table 9 reports the weighted mean abundances of all elements studied in the M2FS spectra of NGC 5824. Star 61005163, whose anomalous abundance pattern will be discussed in great detail in later sections, is omitted from the means presented in Table 9.

8.1 Comparing Abundances Derived from M2FS and MIKE Spectra

Figure 5 compares the abundance ratios derived from M2FS and MIKE spectra for the two stars in common, 42009955 and 61005163. In general, there is superb agreement. The most significant disagreement occurs for the [Mg/Fe] ratio, where the M2FS ratio is lower by 0.43 ± 0.16 dex than the MIKE ratio, on average. Only one Mg I line, at 4571.10 Å, is covered in the M2FS spectra. This line originates from the ground level of the Mg I atom, whereas all other Mg I lines typically studied in metal-poor giants originate from levels at ≈ 2.7 or ≈ 4.3 eV (see, e.g., Table 8 of Roederer et al. 2014a). The direction of the offset we identify is consis-

Table 6. Mean Abundances in Individual Stars, As Derived from the M2FS Spectra

Species	Star	N_{lines}	$\log \epsilon$	[Fe I/H]	σ_{stat}	σ_{tot}	σ_{neut}	σ_{ions}
Fe I	11001198	18	5.11	-2.39	0.04	0.19
Fe I	12001300	18	5.28	-2.22	0.04	0.19
Fe I	21000267	22	5.16	-2.34	0.04	0.19
Fe I	21000688	17	5.11	-2.39	0.04	0.19
Fe I	41000940	16	5.09	-2.41	0.05	0.19

The complete version of Table 6 is available in machine-readable format in the Supplementary Information found in the online edition of the journal. Only a small portion is shown here to illustrate its form and content.

Table 7. Mean Abundances in Star 42009955, As Derived from the MIKE Spectrum

Species	N_{lines}	$\log \epsilon$	[X/Fe] ^a	σ_{stat}	σ_{tot}	σ_{neut}	σ_{ions}
Fe I	117	+5.11	-2.39	0.06	0.19	0.00	0.00
Fe II	10	+5.48	-2.02	0.07	0.10	0.00	0.00
Li I	1	< -0.75	< -1.62
C (CH)	1	+5.25	-1.16	0.15	0.25	0.18	0.18
N (CN)	1	+7.20	+1.39	0.25	0.32	0.27	0.27
O I	3	< +7.00	< +0.70
Na I	4	+4.40	+0.55	0.13	0.22	0.14	0.20
Mg I	4	+5.28	+0.07	0.06	0.21	0.09	0.18
Al I	4	+5.14	+1.08	0.09	0.20	0.11	0.18
Si I	3	+5.95	+0.83	0.17	0.25	0.19	0.24
K I	1	+2.90	+0.26	0.12	0.25	0.15	0.23
Ca I	12	+4.21	+0.26	0.11	0.22	0.12	0.20
Sc II	7	+1.27	+0.14	0.05	0.09	0.17	0.09
Ti I	17	+2.53	-0.03	0.04	0.19	0.07	0.17
Ti II	13	+3.27	+0.33	0.05	0.10	0.16	0.09
V I	10	+1.38	-0.16	0.11	0.21	0.13	0.20
V II	1	+2.07	+0.16	0.19	0.23	0.26	0.23
Cr I	14	+2.96	-0.29	0.05	0.20	0.08	0.18
Cr II	4	+3.80	+0.18	0.05	0.10	0.18	0.09
Mn I	4	+2.64	-0.40	0.07	0.19	0.09	0.17
Co I	3	+2.74	+0.14	0.17	0.25	0.18	0.24
Ni I	7	+3.81	-0.02	0.04	0.18	0.07	0.17
Cu I	1	+1.28	-0.52	0.08	0.20	0.10	0.18
Zn I	2	+2.58	+0.41	0.04	0.18	0.07	0.16
Rb I	0	< +1.45	< +1.32
Sr II	2	+0.89	+0.04	0.17	0.20	0.19	0.20
Y II	7	-0.16	-0.35	0.06	0.09	0.17	0.09
Zr II	6	+0.77	+0.21	0.06	0.10	0.17	0.09
Mo I	1	-0.30	+0.21	0.14	0.23	0.15	0.22
Ba II	3	-0.14	-0.31	0.06	0.11	0.16	0.10
La II	11	-0.94	-0.03	0.06	0.10	0.18	0.10
Ce II	14	-0.63	-0.19	0.05	0.10	0.18	0.09
Pr II	3	-1.31	-0.02	0.05	0.09	0.18	0.09
Nd II	23	-0.63	-0.03	0.06	0.10	0.18	0.10
Sm II	15	-0.89	+0.17	0.05	0.10	0.18	0.09
Eu II	5	-1.26	+0.24	0.08	0.11	0.17	0.10
Gd II	1	-0.66	+0.29	0.06	0.10	0.18	0.10
Tb II	1	-1.70	+0.02	0.11	0.14	0.21	0.14
Dy II	3	-0.63	+0.29	0.06	0.10	0.18	0.09
Er II	1	-0.84	+0.26	0.28	0.29	0.33	0.29
Hf II	2	-0.76	+0.41	0.13	0.16	0.22	0.15
Pb I	1	-0.23	+0.12	0.18	0.25	0.19	0.24
Th II	1	< -1.60	< +0.36

^a [Fe/H] is given for Fe I and Fe II

Table 8. Mean Abundances in Star 61005163, As Derived from the MIKE Spectrum

Species	N_{lines}	$\log \epsilon$	$[\text{X}/\text{Fe}]^a$	σ_{stat}	σ_{tot}	σ_{neut}	σ_{ions}
Fe I	124	+5.21	-2.29	0.06	0.20	0.00	0.00
Fe II	10	+5.58	-1.92	0.07	0.10	0.00	0.00
Li I	1	< -0.48	< -1.45
C (CH)	1	+6.40	-0.11	0.15	0.25	0.18	0.18
N (CN)	1	+6.70	+0.79	0.25	0.32	0.27	0.27
O I	3	+7.89	+1.50	0.11	0.21	0.13	0.19
Na I	1	+3.92	-0.03	0.13	0.22	0.15	0.21
Mg I	4	+5.77	+0.47	0.07	0.21	0.09	0.19
Al I	3	< +4.37	< +0.21
Si I	3	+6.10	+0.89	0.17	0.24	0.18	0.23
K I	1	+2.95	+0.21	0.12	0.25	0.15	0.23
Ca I	12	+4.32	+0.27	0.11	0.22	0.12	0.20
Sc II	7	+1.25	+0.01	0.05	0.09	0.18	0.09
Ti I	15	+2.62	-0.04	0.04	0.20	0.08	0.18
Ti II	13	+3.35	+0.32	0.05	0.10	0.17	0.09
V I	10	+1.50	-0.13	0.11	0.21	0.13	0.20
V II	0
Cr I	14	+3.11	-0.24	0.04	0.20	0.08	0.18
Cr II	3	+3.82	+0.10	0.05	0.09	0.18	0.09
Mn I	4	+2.70	-0.44	0.06	0.19	0.09	0.17
Co I	3	+2.71	+0.02	0.18	0.25	0.19	0.24
Ni I	7	+3.92	-0.00	0.04	0.18	0.08	0.16
Cu I	1	+1.31	-0.59	0.08	0.21	0.10	0.19
Zn I	2	+2.71	+0.45	0.04	0.18	0.07	0.16
Rb I	0	< +1.25	< +1.02
Sr II	1	+1.08	+0.13	0.16	0.19	0.19	0.19
Y II	8	+0.13	-0.16	0.06	0.09	0.17	0.09
Zr II	6	+0.87	+0.21	0.06	0.09	0.17	0.09
Mo I	0
Ba II	3	+0.83	+0.56	0.05	0.12	0.14	0.12
La II	17	-0.35	+0.46	0.05	0.09	0.17	0.08
Ce II	18	+0.13	+0.47	0.05	0.09	0.17	0.08
Pr II	4	-0.78	+0.42	0.07	0.10	0.18	0.09
Nd II	26	-0.02	+0.47	0.05	0.09	0.17	0.08
Sm II	16	-0.59	+0.37	0.04	0.09	0.18	0.09
Eu II	5	-1.21	+0.18	0.08	0.11	0.18	0.10
Gd II	2	-0.37	+0.48	0.05	0.09	0.18	0.09
Tb II	1	-1.55	+0.07	0.11	0.14	0.21	0.14
Dy II	4	-0.31	+0.51	0.07	0.10	0.18	0.10
Er II	1	-0.45	+0.55	0.28	0.29	0.33	0.29
Hf II	2	-0.58	+0.49	0.10	0.13	0.20	0.12
Pb I	1	+0.76	+1.01	0.06	0.23	0.12	0.21
Th II	0

^a $[\text{Fe}/\text{H}]$ is given for Fe I and Fe II

tent with expectations that the ground level of Mg I may experience substantial overionization relative to the LTE level populations (Asplund 2005). The non-LTE calculations of Shimanskaya, Mashonkina, & Sakhibullin (2000) confirm this, although they do not extend to stars cool enough to justify applying corrections to our data. We derive Mg abundances from three other Mg I lines in the MIKE spectra. The Mg I line at 4571 Å also gives abundances lower than these other three lines by 0.41 dex, on average, confirming that our M2FS measurements are not uniquely in error. We caution that the $[\text{Mg}/\text{Fe}]$ ratios reported in Tables 6 and 9 are likely to be lower by ≈ 0.4 dex than $[\text{Mg}/\text{Fe}]$ ratios derived from other Mg I lines.

The $[\text{Ni}/\text{Fe}]$ ratios are both mildly different in these two sets of spectra, where the M2FS ratio is lower than the MIKE ratio by 0.19 ± 0.12 dex. Two Ni I lines, at 4470.48 and 4604.99 Å, have been used in both sets of spectra of both stars. The abundances derived from them agree to 0.07 dex or better. Abundances derived from these lines in the MIKE spectra are lower by 0.18 dex, on average, than the abundances derived from the five other Ni I lines in each star. This indicates that our M2FS Ni abundance determinations are themselves not in error, just as we have found in the case of Mg. No non-LTE calculations are available for Ni lines, to the best of our knowledge; however, the results of Wood et al. (2014a) suggest that any non-LTE effects on

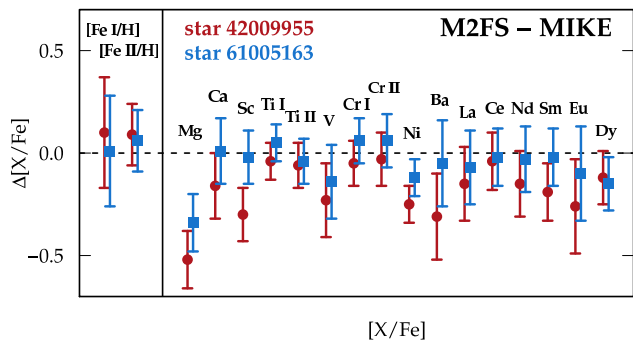


Figure 5. Comparison of abundance ratios derived from M2FS and MIKE spectra for the two stars in common. Red circles indicate star 42009955, and blue squares indicate star 61005163. The dotted line marks a difference of zero.

neutral Ni are minimal, at least in metal-poor subgiants. The cause of the Ni offset is unclear at present. We caution that the $[\text{Ni}/\text{Fe}]$ ratios reported in Tables 6 and 9 are likely to be lower by ≈ 0.2 dex than $[\text{Ni}/\text{Fe}]$ ratios derived from other Ni I lines.

9 THE METALLICITY OF NGC 5824 AND THE POSSIBILITY OF INTERNAL DISPERSION

9.1 Comparison to Da Costa et al. Metallicities

We compare our derived metallicities, inferred from individual Fe II lines in 26 stars in NGC 5824, with those calculated by Da Costa et al. (2014), inferred from a calibration of the Ca II near-infrared triplet EWs. Da Costa et al. did not report metallicities for individual stars, so we follow their procedure using the calibration given by Saviane et al. (2012). We estimate uncertainties on the Da Costa et al. metallicities using a Monte Carlo approach.

Figure 6 illustrates the metallicity distribution for stars in NGC 5824. The hatched dark blue histogram represents metallicities derived by us. The black line represents the full sample of 108 stars examined by Da Costa et al. (2014), and the light blue histogram represents the subset of 26 stars in common to both studies. Our mean metallicities derived from Fe I and Fe II are different by 0.44 dex, but both have a standard deviation of 0.08 dex. The metallicities derived from Fe II lines are in much better agreement with those of Da Costa et al. and an external metallicity scale (Section 9.4), so we prefer these values.

A small offset in $[\text{Fe}/\text{H}]$ is present between our work and that of Da Costa et al. (2014). For the 26 stars in common, our $[\text{Fe}/\text{H}]$ values derived from Fe II lines are higher by 0.08 ± 0.02 dex. Part of this offset may be explained by the slightly lower value of $[\text{Ca}/\text{Fe}]$ that we have derived for NGC 5824 relative to the other metal-poor clusters that Saviane et al. (2012) used to derive their calibration. We find $[\text{Ca}/\text{Fe}] = +0.20 \pm 0.02$, while Gratton et al. (2004) reported a mean of $[\text{Ca}/\text{Fe}] = +0.25 \pm 0.02$ for 28 clusters with $[\text{Fe}/\text{H}] < -1$, including many used by Saviane et al. Da Costa et al. note that the uncertainty in the mean metallicity derived for NGC 5824 using their Ca triplet calibra-

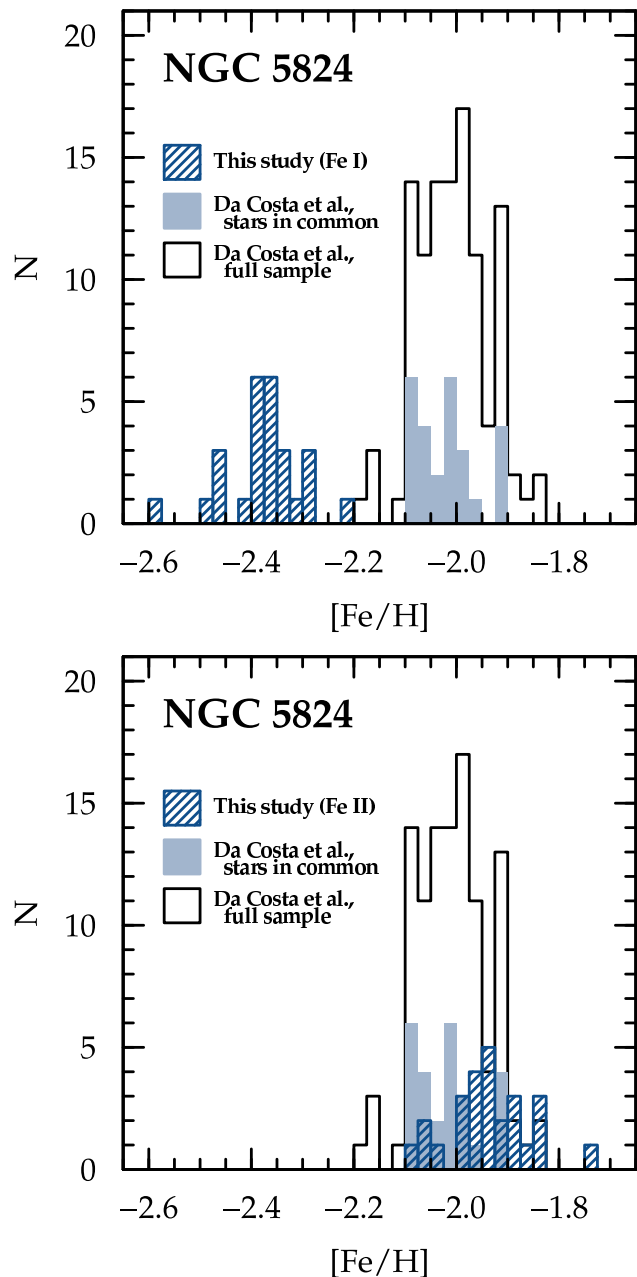


Figure 6. The metallicity distribution function of NGC 5824. The dark blue hatched histogram represents metallicities derived by us using Fe I lines (top panel) or Fe II lines (bottom panel) in 26 stars. The unfilled black histogram represents metallicities for the full sample of 108 stars examined by Da Costa et al. (2014). The filled light blue histogram represents the subset of 26 stars from Da Costa et al. that are common to our study.

tion, $[\text{Fe}/\text{H}] = -2.01 \pm 0.13$, is dominated by the calibration relation itself.

9.2 Tests of Internal Metallicity Dispersion

Figure 7 compares our results with those of Da Costa et al. (2014). The metallicities derived by Da Costa et al. and us are inferred from independent spectral features. We might expect to find a correlation in Figure 7 if $[\text{Ca}/\text{Fe}]$ is rela-

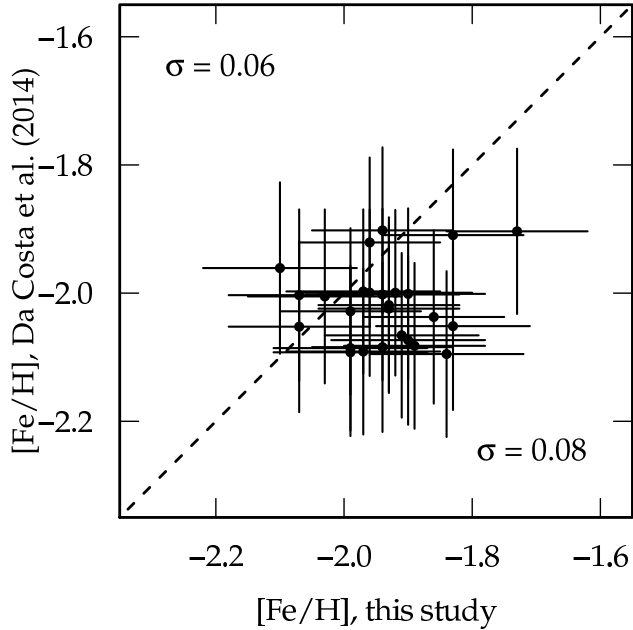


Figure 7. Comparison of metallicities derived in our study (using Fe II lines) with those inferred from Ca II triplet EWs measured by Da Costa et al. (2014). The dashed line represents a one-to-one correlation.

tively constant and there is an intrinsic metallicity dispersion within NGC 5824 that exceeds the observational uncertainties. The p -value for the linear correlation coefficient is 0.52, affirming our visual impression that no significant correlation is found.

Figure 8 illustrates our observed metallicity distributions in NGC 5824, which are equivalent to the hatched blue histograms in Figure 6. Our metallicities have standard deviations of 0.08 dex derived from either Fe I or Fe II lines. The black curves in Figure 8 illustrate normal distributions with a mean metallicity of -2.38 (for Fe I) or -1.94 (for Fe II) and standard deviations of 0.08 dex. We estimate the formal widths of the $[\text{Fe}/\text{H}]$ distributions that would be expected given errors in the input quantities used to calculate T_{eff} and $\log g$. We assume $\sigma_{T_{\text{eff}}} = 145$ K, $\sigma_{\log g} = 0.14$ dex, and $\sigma_{v_t} = 0.1$ km s $^{-1}$, as estimated in Section 6. Most of the errors on the other input quantities in the $\log g$ calculation in Section 6 are systematic, so they affect all stars similarly. We ignore the errors in these quantities for now. For a given star, we use 1000 realizations of model atmosphere parameters drawn from normal distributions with these standard deviations, and we rederive the $[\text{Fe}/\text{H}]$ ratios. The standard deviations of the resulting $[\text{Fe}/\text{H}]$ distributions vary somewhat with T_{eff} , but the median values are ≈ 0.15 dex for both Fe I and II. This value is illustrated by the blue curves in Figure 8.

It is apparent from Figure 8 that the expected distributions overestimate the observed widths by about a factor of two. This likely signals that we have overestimated the errors on the model atmosphere parameters. The largest source of error that contributes to the width in the predicted $[\text{Fe}/\text{H}]$ distribution is $\sigma_{T_{\text{eff}}}$, which enters the calculation twice: once through T_{eff} itself, and once through $4\log T_{\text{eff}}$ in the $\log g$ formula. The Alonso et al. (1999) $V - I$ color- T_{eff} calibration

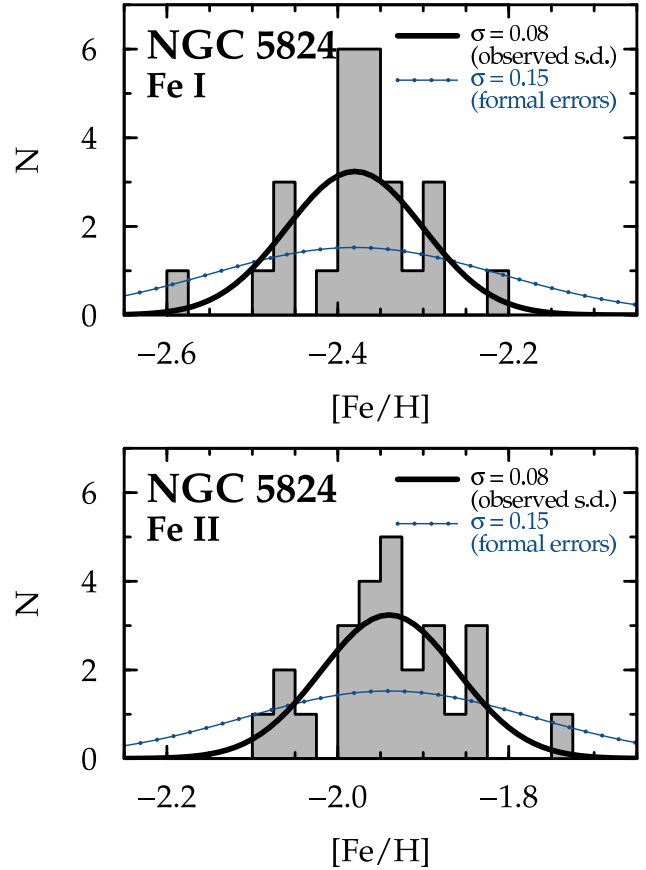


Figure 8. Observed metallicity distributions (gray shaded histograms) in NGC 5824. The top panel shows the results from Fe I lines, and the bottom panel shows the results from Fe II lines. The bold black line represents a normal distribution with mean $[\text{Fe}/\text{H}] = -2.38$ (Fe I) or $[\text{Fe}/\text{H}] = -1.94$ (Fe II) and standard deviation 0.08, which is equivalent to the standard deviation of the derived metallicities for both Fe I and II. The studded blue line represents a normal distribution with mean $[\text{Fe}/\text{H}] = -2.38$ (Fe I) or $[\text{Fe}/\text{H}] = -1.94$ (Fe II) and standard deviation 0.15, which is equivalent to the formal error distributions predicted for our data. All distributions are normalized to the areas of the observed histograms.

has an intrinsic scatter of 125 K. If we arbitrarily assume zero scatter in this calibration, $\sigma_{T_{\text{eff}}}$ decreases to 74 K (reflecting quantities related to the photometry), and $\sigma_{[\text{Fe}/\text{H}]}$ decreases to 0.09 dex, close to the observed value.

We compare the results with another T_{eff} scale to assess whether this arbitrary assumption is plausible. The $V - I_c$ color- T_{eff} relation of Casagrande et al. (2010) has an intrinsic scatter of only 59 K. This scale was calibrated using dwarfs, but Casagrande et al. (2014) have shown that it is also applicable to giants. The Casagrande et al. calibration predicts T_{eff} values warmer than the Alonso et al. scale by 85 K for these stars. The standard deviation of the residuals between the two scales is only 3 K, however. The excellent agreement of these two scales—zeropoint aside—offers reassurance that the statistical errors on T_{eff} may be smaller than assumed.

Our tests indicate that no reasonable assumptions for the errors in T_{eff} , $\log g$, or v_t can produce a predicted $[\text{Fe}/\text{H}]$ distribution for either Fe I or II narrower than the observed

one. Furthermore, we have assumed during these calculations that the measurement errors on the EWs are zero, which also would lead us to underestimate the widths of the predicted $[\text{Fe}/\text{H}]$ distributions. We conclude that there is no internal metallicity dispersion among the stars observed in NGC 5824. We estimate a systematic uncertainty of 0.10 dex in the mean metallicity when sources of systematic uncertainty are considered.

We do not find evidence in our data for the metallicity spread reported by Da Costa et al. (2014), but that study would also not have found evidence for a metallicity spread if they were restricted to the 26 stars studied by us. The dispersion in their metallicities of these 26 stars, 0.06 dex, is equivalent to the expected error distribution. This value is smaller than the FWHM of the distribution shown in Figure 12 of Da Costa et al., 0.16 dex, or the inner-quartile range, 0.10 dex, reported based on their full sample of 108 stars.

Figure 9 illustrates the Da Costa et al. metallicities as a function of V magnitude. Open circles represent their full sample, and filled circles represent stars in common with our sample. Stars that contribute to the tails of their metallicity distribution have $V > 17$, where we have no stars in common. One explanation is that this simply reflects the increasing measurement errors for fainter stars. If, however, NGC 5824 has an intrinsic metallicity spread, the stars with higher metallicities may not occupy the upper RGB, and our observations would be biased against them. Stars with lower metallicities would generally not be fainter and should be found in our sample, so this explanation may only tell part of the story. The radial distributions of our sample and the full Da Costa et al. sample are only mildly different, with the Da Costa et al. sample being slightly more extended than ours. The two-sided Kolmogorov-Smirnov test returns a p -value of 0.12 when applied to the cumulative radial distributions of these samples, and the Cramer-von Mises test returns a p -value of 0.044. If lower metallicity stars are found at greater radii, on average, this could explain the tail to lower metallicities.

Another partial explanation for the range of Ca II triplet strengths found by Da Costa et al. (2014) could be an opacity effect caused by the Mg-deficient stars. Mucciarelli et al. (2012) noted that the most Mg-deficient stars in NGC 2419 were preferentially those with the highest $[\text{Ca}/\text{H}]$ ratios. Mg is one of the dominant donors of electrons to form the H^- ion, the primary source of continuous opacity in late-type metal-poor stars. Mucciarelli et al. contend that the continuous opacity decreases when Mg is depleted, leading to stronger Ca II lines even though the Ca abundance is constant. The saturated Ca II triplet lines are partially formed in layers of the atmosphere most sensitive to the electron pressure (see Figure 7 of Mucciarelli et al.), whereas lines on the weak part of the curve of growth are minimally-affected. Figure 10 compares the Da Costa et al. metallicities derived from Ca II triplet lines with the $[\text{Mg}/\text{Fe}]$ ratios derived by us. We estimate the significance of the correlation in Figure 10 by calculating the p -values for the Spearman and Pearson coefficients from 1000 resamplings of the $[\text{Mg}/\text{Fe}]$ and Ca II triplet metallicity distributions given their observed errors. The median p -values are 0.40 and 0.37, respectively, indicating that the correlation is not significant. Regardless, depletions in Mg could not fully explain the situation, as noted

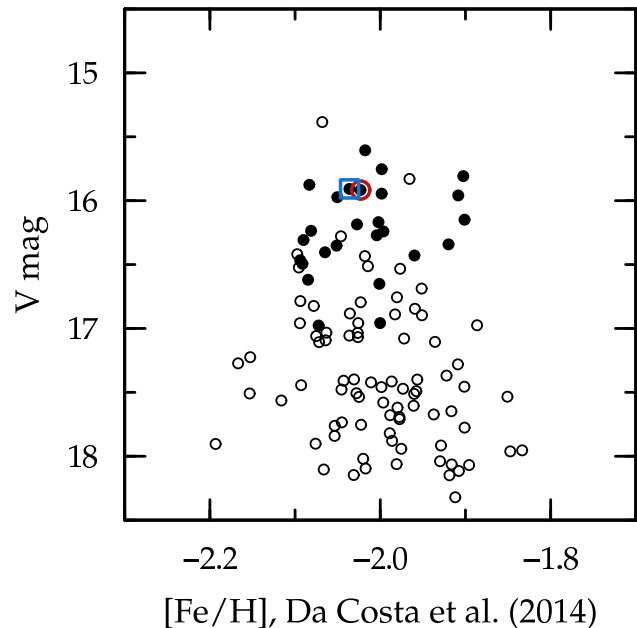


Figure 9. Metallicities for the Da Costa et al. (2014) sample inferred from the Ca II triplet EWs. Open circles denote all 108 stars in their sample, and filled circles mark the 26 stars in common with us. The red circle marks star 42009955, and the blue square marks star 61005163.

in Section 1. Da Costa et al. (2009) discovered an intrinsic dispersion in the strengths of the Ca II triplet in M22 red giants, similar to that found in NGC 5824. However, no significant depletions in $[\text{Mg}/\text{Fe}]$ or other electron donors are found in M22 (Marino et al. 2011). No satisfactory explanation has been found for the Da Costa et al. result in M22, and the possibility of a metallicity spread in NGC 5824 is unresolved by our data.

9.3 A Differential Analysis of Stars 42009955 and 61005163

We use a differential approach to examine whether there may be abundance variations between the two stars observed with MIKE, 42009955 and 61005163. These two stars are highlighted in Figures 9 and 10. There are 101 Fe I lines in common, 10 Fe II lines, 12 Ca I lines, 14 Ti I lines, 13 Ti II lines, 14 Cr I lines, and 7 Ni I lines. The line-by-line differentials, in the sense of star 42009955 minus star 61005163, are $\delta[\text{Ca}/\text{Fe}] = -0.020 \pm 0.027$, $\delta[\text{Ti I}/\text{Fe}] = -0.036 \pm 0.039$, $\delta[\text{Ti II}/\text{Fe}] = -0.038 \pm 0.061$, $\delta[\text{Cr}/\text{Fe}] = +0.008 \pm 0.023$, $\delta[\text{Ni}/\text{Fe}] = +0.007 \pm 0.021$. All of the errors reported here are statistical only, and none of these differences are significant. These ratios are also robust and consistent with no difference when Fe is removed from the construction: $\delta[\text{Ca}/\text{Ni}] = -0.028 \pm 0.031$, for example. We conclude that the abundances of the Fe-group elements (including Ca and Ti) are constant in these two stars.

The overall metallicities are significantly different when considering Fe I lines, $\delta[\text{Fe I}/\text{H}] = -0.129 \pm 0.010$, but they are not significantly different when considering Fe II lines, $\delta[\text{Fe II}/\text{H}] = -0.059 \pm 0.057$. As noted previously, other studies (e.g., Mucciarelli et al. 2015b) have pointed out that Fe I lines may be a poor representation of the Fe abundance

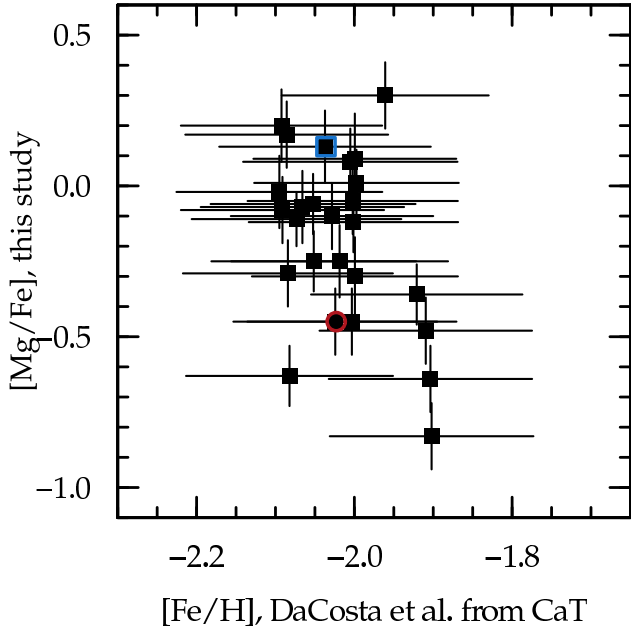


Figure 10. Our $[\text{Mg}/\text{Fe}]$ ratios as a function of the $[\text{Fe}/\text{H}]$ inferred from the Ca II triplet (CaT) measurements of Da Costa et al. (2014). The red circle marks star 42009955, and the blue square marks star 61005163.

in cool, metal-poor giants in globular clusters. Whatever the cause of this effect, Mucciarelli et al. have shown that it may be most pronounced in stars that show the s -process enhancement, like star 61005163 (see Section 10.3). Fe II lines may be more reliable. We conclude that this differential analysis does not offer compelling evidence for metallicity differences between stars 42009955 and 61005163.

Our referee notes, correctly, that this technique may not be strictly valid if the He abundance or total abundance of C, N, and O differs between these two stars. Sbordone et al. (2011) have shown that stars with the same color but differing He or total C, N, and O abundances will separate into different sequences using broadband optical photometry. Our method for deriving $\log g$ would then need to be refined for the additional sequence. We cannot evaluate the He abundances or total abundance of C, N, and O in these two stars, and broadband optical photometry has not yet revealed multiple sequences on the red giant branch of NGC 5824 (Piotto et al. 2002). Evidence suggests, however, that NGC 5824 may be a good candidate to search for the presence of He variations (Section 10.1), which have been detected in every cluster investigated (Milone 2015), so this matter is unresolved at present.

9.4 The Metallicity of NGC 5824 on the Koch & McWilliam Scale

Koch & McWilliam (2008) have established a globular cluster metallicity scale based on a differential abundance analysis with the K-giant Arcturus (α Boo), whose temperature is known to better than 30 K. Koch & McWilliam (2011) placed the metal-poor cluster NGC 6397 on this scale, finding $[\text{Fe}/\text{H}] = -2.10 \pm 0.02$ (statistical) ± 0.07 (systematic). For three unblended Fe II lines in common between

three stars in NGC 6397 (stars 7230, 8958, and 13414) and our MIKE spectra of stars 42009955 and 61005163, we find a mean line-by-line offset of $+0.23 \pm 0.04$ dex in the sense of NGC 5824 minus NGC 6397. Relative to the Koch & McWilliam metallicity of NGC 6397, NGC 5824 has a metallicity of $[\text{Fe}/\text{H}] = -1.87 \pm 0.04$ (statistical) ± 0.07 (systematic). This is in reasonable agreement with the metallicity we have derived, $[\text{Fe}/\text{H}] = -1.94 \pm 0.02$ (statistical) ± 0.10 (systematic).

10 DISCUSSION

10.1 Light Elements

Mg is the only light element that is sometimes found to vary within globular clusters that is covered by our M2FS spectra. Nevertheless, the dispersion in the $[\text{Mg}/\text{Fe}]$ ratios, 0.28 dex, far exceeds that of any other α - or Fe-group element. The inner quartile range of $[\text{Mg}/\text{Fe}]$ ratios is 0.35 dex, and the full range is 1.1 dex. Recall (Section 8.1) that the $[\text{Mg}/\text{Fe}]$ ratios derived from the M2FS spectra may be systematically underestimated by ≈ 0.4 dex, but the star-to-star dispersion should be reliable.

Large star-to-star variations in $[\text{Mg}/\text{Fe}]$ have been found in some luminous, metal-poor clusters, including ω Cen (e.g., Norris & Da Costa 1995; Smith et al. 2000), M3 (Snedden et al. 2004; Johnson et al. 2005), M13 (Pilachowski et al. 1996; Shetrone 1996; Kraft et al. 1997), M15 (Snedden et al. 1997; Carretta et al. 2009b), NGC 2419 (Cohen & Kirby 2012; Mucciarelli et al. 2012), NGC 2808 (Carretta et al. 2009b; Carretta 2014), NGC 4833 (Carretta et al. 2014; Roederer & Thompson 2015), NGC 6752 (Gratton et al. 2001; Yong et al. 2003), and possibly M62 (Yong et al. 2014a) and M92 (Shetrone 1996). Some of these clusters are also suspected to contain groups of stars with substantial He enhancements (ω Cen: Piotto et al. 2005, King et al. 2012; M62: Milone 2015; NGC 2419: Di Criscienzo et al. 2011; NGC 2808: Piotto et al. 2007, Milone et al. 2015a; NGC 6752: Milone et al. 2013). NGC 5824, too, is luminous, metal-poor, and shows a large internal $[\text{Mg}/\text{Fe}]$ dispersion. The relatively large dispersion in $[\text{Mg}/\text{Fe}]$ distinguishes NGC 5824 from other clusters with complex heavy-element abundance patterns, where the $[\text{Mg}/\text{Fe}]$ dispersions range from 0.04 dex to 0.15 dex (M2, M19, M22, NGC 1851, NGC 5286; Carretta et al. 2011; Marino et al. 2011, 2015; Yong et al. 2014b; Johnson et al. 2015b). NGC 5824 may be a good candidate to search for the presence of internal He variations.

Our MIKE spectra of stars 42009955 and 61005163 include lines of O I, Na I, Mg I, and Al I. These are illustrated in Figure 11. Examination of the spectra reveal the usual light element abundance variations found within globular clusters. Star 61005163 has relatively strong O I lines, weak Na I lines, strong Mg I lines, and non-detected Al I lines. Star 42009955, in contrast, has non-detected O I lines, relatively strong Na I lines, weak Mg I lines, and strong Al I lines. The abundances reported in Tables 7 and 8 quantitatively confirm these impressions.

Si and K have also been shown to occasionally participate in the high-temperature p -capture reactions

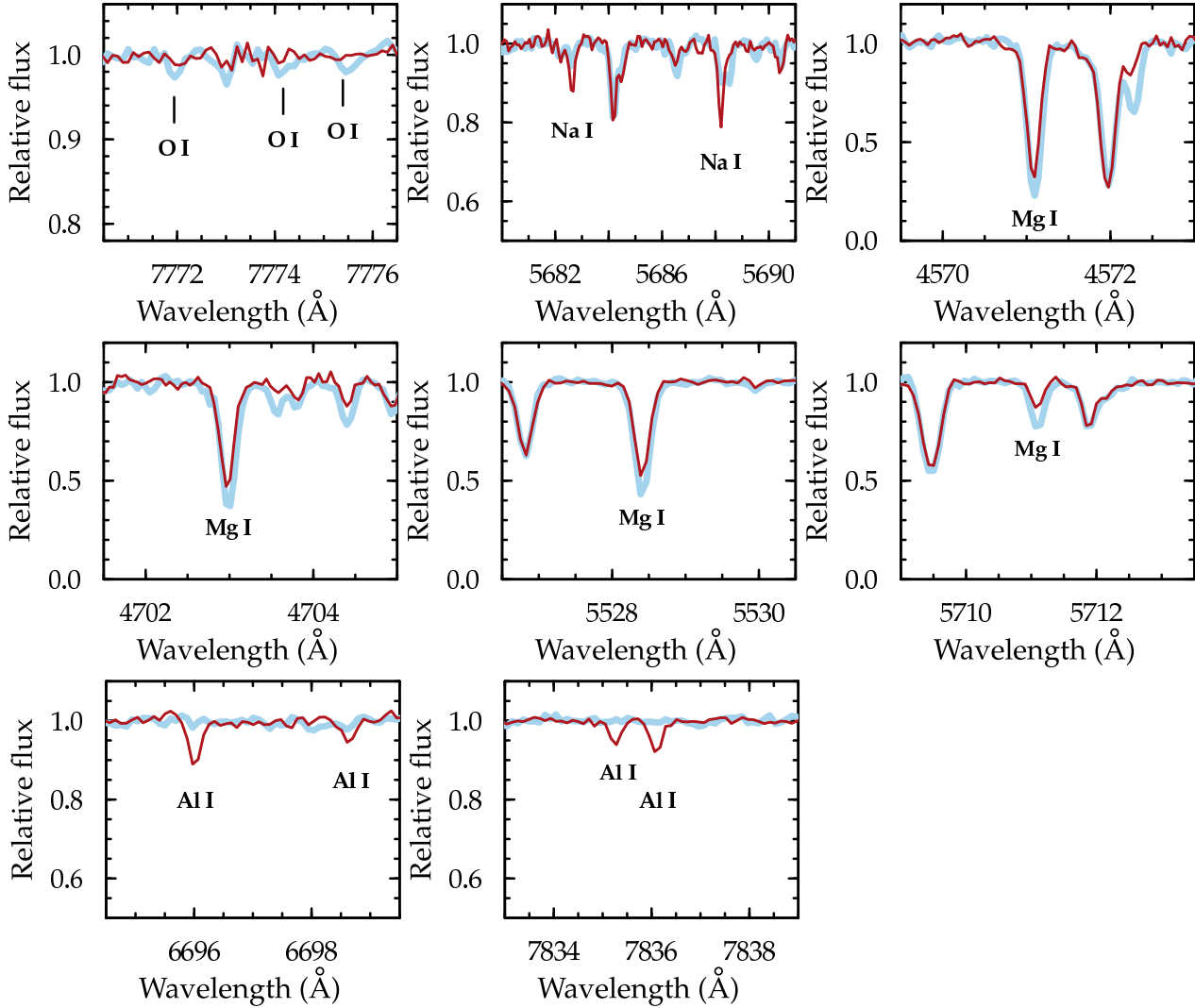


Figure 11. Selections of the MIKE spectra of stars 42009955 (thin red line) and 61005163 (bold blue line) around several O I, Na I, Mg I, and Al I lines.

that produce the light element abundance variations in globular clusters (Yong et al. 2005; Carretta et al. 2009b, 2013b; Cohen & Kirby 2012; Mucciarelli et al. 2012, 2015a; Ventura et al. 2012; Mészáros et al. 2015). These two elements are only covered in the MIKE spectra. In both cases, the $[\text{Si}/\text{Fe}]$ and $[\text{K}/\text{Fe}]$ ratios are in agreement. These two stars show variations in the $[\text{O}/\text{Fe}]$, $[\text{Na}/\text{Fe}]$, $[\text{Mg}/\text{Fe}]$, and $[\text{Al}/\text{Fe}]$ ratios, so $[\text{Si}/\text{Fe}]$ and $[\text{K}/\text{Fe}]$ may not vary substantially within NGC 5824.

CH and CN molecular features are detected in our two MIKE spectra. $[\text{C}/\text{Fe}]$ is subsolar and $[\text{N}/\text{Fe}]$ is supersolar in both stars, which is consistent with the scenario where C is depleted and converted to N as stars evolve up the RGB. We estimate the natal $[\text{C}/\text{Fe}]$ ratios in these two stars using the results of Placco et al. (2014), who provide a set of corrections based on stellar evolution models that relate the current $[\text{C}/\text{Fe}]$ ratio of a star on the RGB to the initial $[\text{C}/\text{Fe}]$ ratio. For star 42009955, the observed $[\text{C}/\text{Fe}] = -1.16$ maps to $[\text{C}/\text{Fe}]_{\text{init}} \approx -0.55$. For star 61005163, the observed $[\text{C}/\text{Fe}] = -0.11$ maps to $[\text{C}/\text{Fe}]_{\text{init}} \approx +0.44$. Neither of these initial $[\text{C}/\text{Fe}]$ ratios would be considered “carbon-

enhanced” by modern definitions (Aoki et al. 2007), which require $[\text{C}/\text{Fe}]_{\text{init}} \geq +0.7$.

For completeness, we note that the Li I line at 6707 Å is covered in our MIKE spectra. Li I is not detected in either star. The upper limits are consistent with the levels of Li-depletion commonly found in other cluster and field stars on the upper RGB (e.g., Gratton et al. 2000; Lind et al. 2009).

10.2 Elements in the Iron Group

Figure 12 compares the mean abundance ratios in NGC 5824 (excluding star 61005163) with those in halo stars of similar metallicity. The gray boxes represent the median \pm one standard deviation of 14 red giant stars in the solar neighborhood with $-2.5 < [\text{Fe}/\text{H}] < -1.5$ (Roederer et al. 2014a). There is superb agreement between the Fe-group elements in NGC 5824 the halo field sample for the nine ratios shown in Figure 12. We conclude that the overall composition of NGC 5824 for elements with $20 \leq Z \leq 28$ (Ca to Ni) is indistinguishable from that of the Galactic halo in the solar neighborhood.

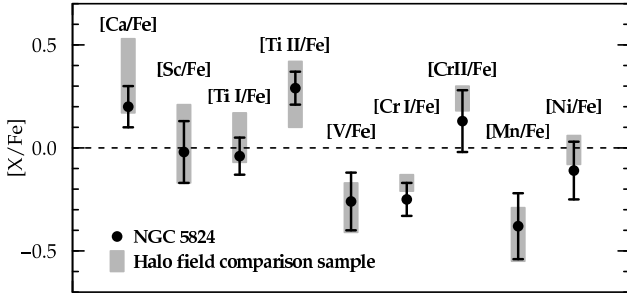


Figure 12. Comparison of abundance ratios in NGC 5824 and a sample of field red giants with similar metallicity. The black points represent the NGC 5824 ratios, derived from the M2FS spectra, and the gray shaded boxes represent the median \pm one standard deviation for the field sample.

Cu has been found to correlate with the s -process enhancement found in other complex, low-metallicity clusters, like M2, M22, and NGC 5286. Zn also correlates with the s -process enhancement in M22. Cu I and Zn I lines are only covered in our MIKE spectra. One star, 42009955 shows no s -process enhancement, while the other, 61005163, does (see Section 10.3). We find no significant differences among the [Cu/Fe] or [Zn/Fe] ratios in these two stars.

10.3 Neutron-Capture Elements

Eight elements heavier than the Fe-group are detectable in our M2FS spectra, and 17 are detectable in our MIKE spectra. The n -capture abundance patterns are virtually identical in 25 of the 26 stars examined, as shown in Figure 13. Each panel in Figure 13 shows the logarithmic abundances in one star. For comparison, a template for the “main” component (Truran et al. 2002) of the r -process pattern is shown. Overall, the patterns observed in NGC 5824 are a close match to the r -process pattern. The [Ba/Eu] ratio is commonly used to quantify the relative contributions of the r - and s -process. In NGC 5824, $\langle [\text{Ba}/\text{Eu}] \rangle = -0.66 \pm 0.05$, in good agreement with the value found in highly r -process-enhanced stars, -0.71 ± 0.05 (Roederer et al. 2014b).

The mean [Eu/Fe] ratio derived from the M2FS spectra, $\langle [\text{Eu}/\text{Fe}] \rangle = +0.11 \pm 0.12$, is somewhat lower than that found in other low-metallicity clusters, $\approx +0.5 \pm 0.2$ (Roederer 2011). This ratio is commonly used to assess the overall enhancement of r -process material in a cluster. Sneden, Pilachowski, & Kraft (2000) found that the n -capture elements in globular cluster M92 are less abundant by ≈ 0.3 dex when compared with M15, another cluster at similar metallicity. That result suggests there may be a genuine, though small, cluster-to-cluster dispersion in the overall abundance of n -capture elements. NGC 5824 may lie at the low end of this dispersion.

Slight overabundances relative to this r -process pattern are detectable for Sr ($Z = 38$), Ba ($Z = 56$), Ce ($Z = 58$), and Nd ($Z = 60$). It is well-known (e.g., McWilliam 1998; Johnson & Bolte 2002) that the ratios between the light (e.g., Sr) and heavy (e.g., Ba or Eu) n -capture elements vary in low-metallicity field stars even when little or no s -process contributions are present. This phenomenon is also observed in globular clusters (e.g., Yong et al. 2014a; Roederer & Thompson 2015), and NGC 5824 appears to be

no exception in this regard. The Ba abundances are derived from a single, saturated line at 4554 Å, and they are highly sensitive to the adopted v_t value. Furthermore, the slight Ba, Ce, and Nd overabundances can be attributed to contributions from both the “weak” and “main” components of the r -process. We would also expect to see significant Pb enhancement if these overabundances come from s -process nucleosynthesis (e.g., Roederer et al. 2010b), since low-metallicity AGB stars are prodigious producers of Pb (e.g., Gallino et al. 1998; Van Eck et al. 2001). The low $\log \epsilon(\text{Pb}/\text{Eu})$ ratio observed in star 42009955 confirms that little or no s -process material is present. We conclude that the n -capture elements in these 25 stars were produced by some form of r -process nucleosynthesis. The r -process is thought to occur in explosive environments like core-collapse supernovae or neutron-star mergers, so this enrichment almost certainly occurred before the present-day stars of NGC 5824 formed.

Figure 14 illustrates the relationships between heavy n -capture elements found in NGC 5824. The 25 stars with only r -process products are shown with red circles. These form a well-defined locus in each panel, with the exception of the Ba abundances, which we have previously noted are especially sensitive to the adopted v_t values. Subtle correlations are apparent among some ratios, like [Ce/Fe] and [Nd/Fe]. This does not signal cosmic star-to-star dispersion within NGC 5824 (cf. Roederer 2011; Cohen 2011). Rather, these correlations are likely due to random uncertainties in the model atmosphere parameters that impact the derived abundances similarly for each element (Roederer & Thompson 2015). We conclude that the n -capture abundance patterns within these 25 stars in NGC 5824 are effectively identical.

The one exception, star 61005163, shows large excesses of Ba, La, Ce, and Nd in the M2FS spectrum. This star is shown by the blue square in Figure 14. Its [Sm/Fe], [Eu/Fe], and [Dy/Fe] ratios are indistinguishable from the other stars. These differences are immediately apparent from visual inspection of the spectra. Figure 15 shows sections of the MIKE spectra of stars 42009955 and 61005163 surrounding some of the n -capture lines. These two stars have identical stellar parameters and metallicities, so differences in their spectra can be attributed to unequal abundances. Most of the absorption lines are formed by Fe-group elements whose abundances are identical in the two stars (Section 10.2), and their line strengths are identical, too. Lines of n -capture elements are marked, and these lines account for nearly all of the differences in the spectra.

Figure 16 shows the n -capture abundance patterns derived from the MIKE spectra of stars 42009955 and 61005163. The metal-poor ([Fe/H] = -2.1) r -process-enhanced standard star BD+17 3248 is shown for comparison. The abundances of most n -capture elements are different between the two stars. No elements have a lower abundance in star 61005163 than in star 42009955. BD+17 3248 is a good match for the elements with $Z \geq 56$ in star 42009955, but not for these elements in star 61005163. We refer to the abundance pattern in star 61005163 as the “ $r + s$ ” pattern, and we refer to the abundance pattern in star 42009955 as the “ r -only” pattern.

Following the procedure outlined in Roederer, Marino, & Sneden (2011) for the two n -capture

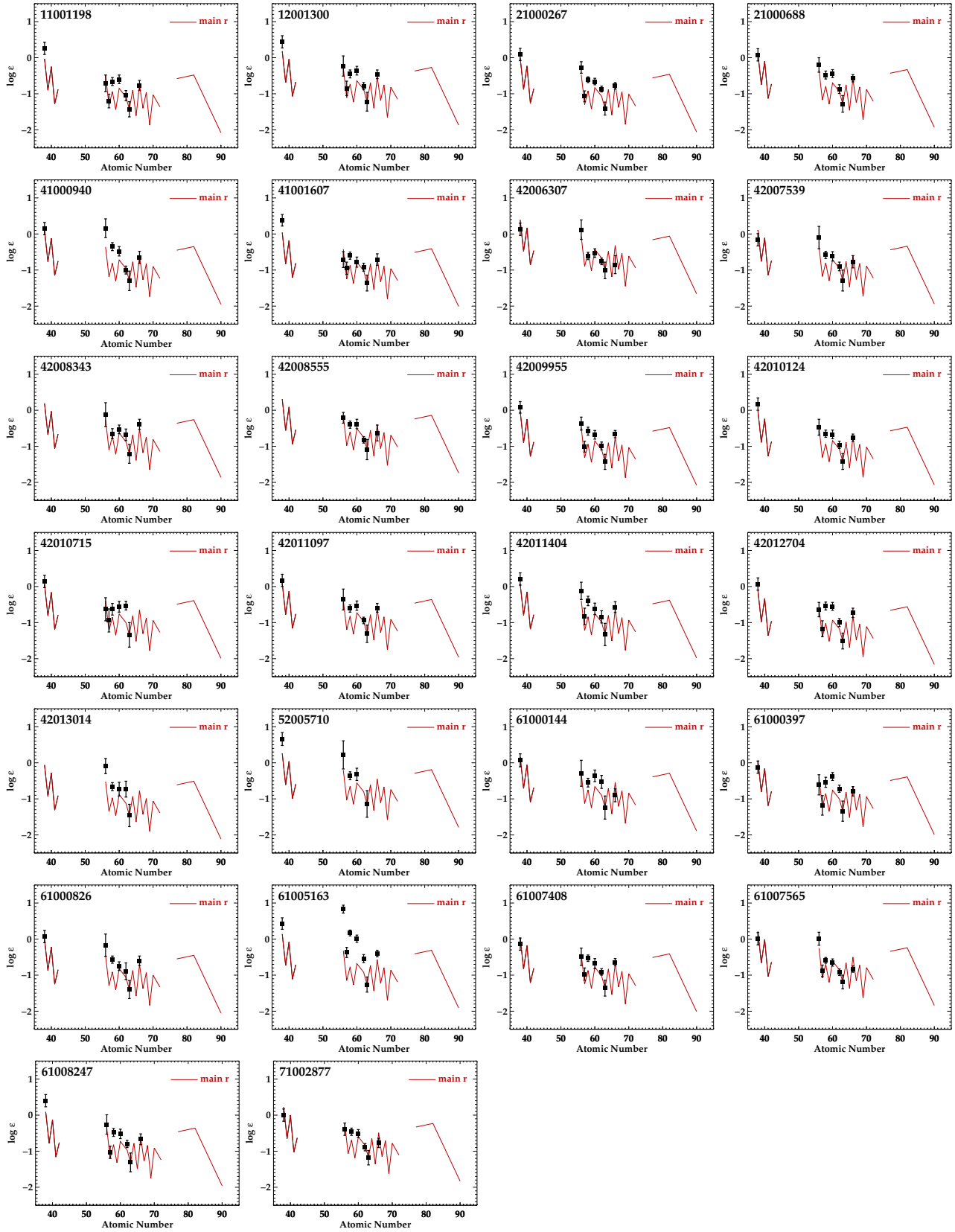


Figure 13. Heavy element abundance patterns derived from M2FS spectra in all 26 stars examined. The red line marks a template for the r -process abundance pattern (the star CS 22892–052; Sneden et al. 2003, 2009; Roederer et al. 2009), which is normalized to the Eu abundance in each star.

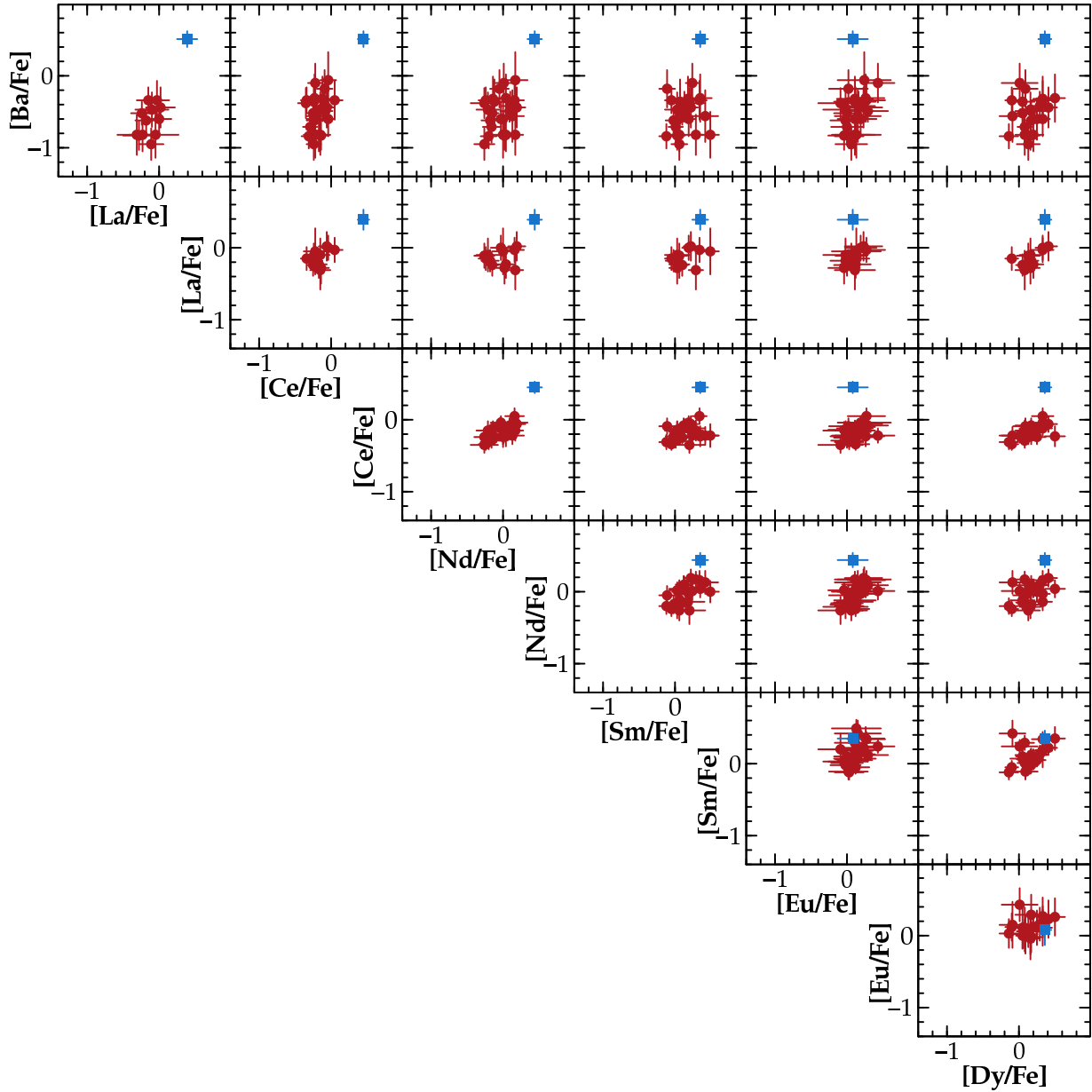


Figure 14. Abundances of heavy n -capture elements in NGC 5824. Red circles mark stars in the r -only group, and the blue square marks star 61005163.

patterns in globular cluster M22, we subtract the abundance pattern in the r -only group from the abundance pattern in the $r + s$ group to reveal the “ s -process residual” pattern. This method assumes that the (r -process) “foundation” is identical in all stars in NGC 5824, but it makes no assumptions about the nucleosynthesis origins of the foundation. The difference between the two stars—the s -process residual—is illustrated in the bottom panel of Figure 16. Note that the abundance differences are largely insensitive to non-LTE effects that affect line formation (for, e.g., Pb; Mashonkina, Ryabtsev, Frebel 2012), since stars 42009955 and 61005163 have identical stellar parameters and metallicities.

An unmistakable correlation emerges when these differences are plotted as a function of the s -process contri-

bution to the solar system abundance of each element, as shown in the bottom panel of Figure 17. Elements with minimal s -process contribution (< 10 per cent; Eu, Tb) to their solar abundances show no difference between the r -only and $r + s$ groups. Elements with major s -process contributions (> 80 per cent; Ba, Ce, Pb) show the largest differences. Other n -capture elements fall between these two extremes. The lone exception, Hf, only deviates from the mean trend by $< 2 \sigma$. We regard this as compelling evidence that s -process nucleosynthesis is responsible for the differences in the abundance patterns between stars 42009955 and 61005163.

To summarize, we find that 25 of the 26 stars observed in NGC 5824 share a common n -capture element abundance pattern consistent with a nucleosynthetic origin in some

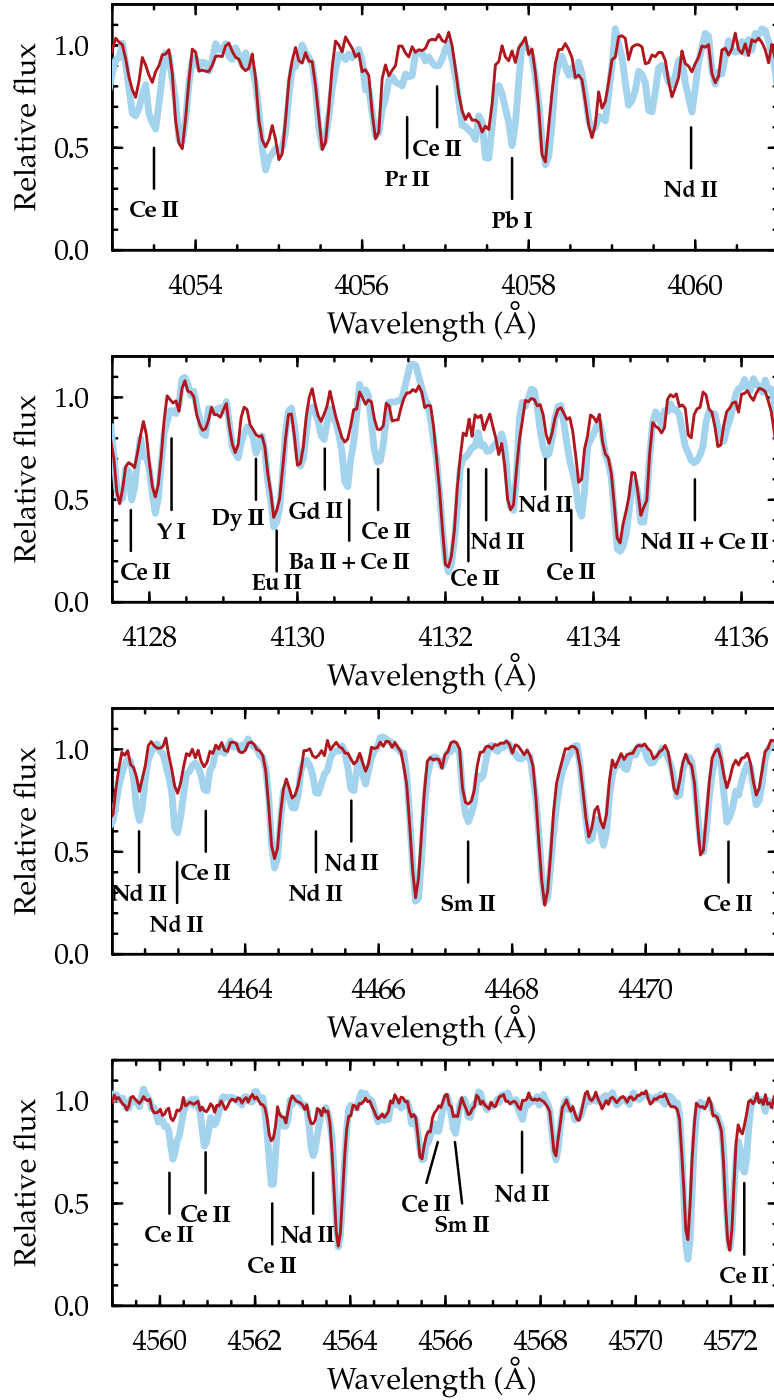


Figure 15. Selections of the MIKE spectra of stars 42009955 (thin red line) and 61005163 (bold blue line) around various lines of n -capture elements. The few differences in the top panel that do not correspond to n -capture element lines are due to differences in the CH abundance.

form of r -process. One of these 26 stars shows substantial amounts of s -process material, as well.

10.4 Natal Enrichment, Self-Enrichment, or Mass Transfer from a Companion?

We have found only one star with an unusual abundance pattern in NGC 5824, which raises the possibility that the composition of the atmosphere of this star does not reflect its

natal composition. In this section, we consider, and dismiss, the possibilities that star 61005163 received its s -process enhancement by self-enrichment or by mass-transfer from a companion star that passed through the AGB phase of evolution. As a reminder, in this context “self-enrichment” refers to the mechanism by which the composition of the surface layers of a star are changed through internal nucleosynthesis and/or mixing episodes, not polluters from one stellar generation enriching other stars in a later generation.

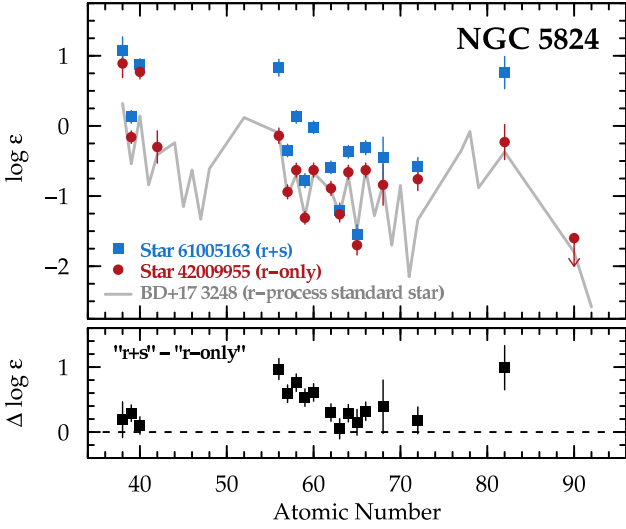


Figure 16. Logarithmic abundances of the n -capture elements in NGC 5824 as derived from the MIKE spectra. In the top panel, blue squares mark star 61005163, and the red circles mark star 42009955. The gray line marks the n -capture element abundance pattern observed in the metal-poor r -process-enhanced standard star BD+17 3248 (Cowan et al. 2002, 2005; Sneden et al. 2009; Roederer et al. 2009, 2010a, 2012a). This pattern is normalized to the Eu abundance. In the bottom panel, the squares mark the offset between the two stars in NGC 5824, characterized as “ $r+s$ minus r -only.” The dashed line represents a difference of zero.

Star 61005163 ($M_{\text{bol}} = -2.76$) is not luminous enough to have produced the observed s -process material through self-enrichment. The latest update to the Full-network Repository of Updated Isotopic Tables & Yields (FRUITY, version 4; Cristallo et al. 2015) database presents physical parameters and s -process yields for AGB stars with initial masses from 1.3 to 6.0 M_{\odot} . The models for low-metallicity stars have $-5.2 < M_{\text{bol}} < -3.5$ during the thermally-pulsing AGB (TP-AGB) phase of evolution, when s -process nucleosynthesis occurs. Several stars in our sample are more luminous than star 61005163, and none shows evidence of s -process enhancement. We therefore discard the possibility that star 61005163 is an intrinsic s -process-enriched AGB star.

Ba enhancement is always accompanied by C enhancement in low-metallicity field stars whenever the Ba enhancement does not originate from r -process nucleosynthesis (e.g., Aoki et al. 2007, Sneden et al. 2008, Allen et al. 2012). Such stars are classified as carbon-enhanced metal-poor stars with s -process enhancement, or CEMP- s (Ryan et al. 2005; Beers & Christlieb 2005). Frequently, these stars are found in binary (or multiple) star systems, as revealed by radial velocity variations. They are presumed to have acquired their carbon and s -process enhancement from a more massive companion that evolved through the AGB phase of evolution and transferred the C and s -process material to the longer-lived star, which we now observe.

Star 61005163 does not exhibit radial velocity variations in our two observations spaced ≈ 2 months apart. This information alone does not exclude the possibility of a companion, since the system could be observed face-on or have a very long ($\gtrsim 10^3$ d) orbital period.

Star 61005163 is not C-enhanced, and it probably was

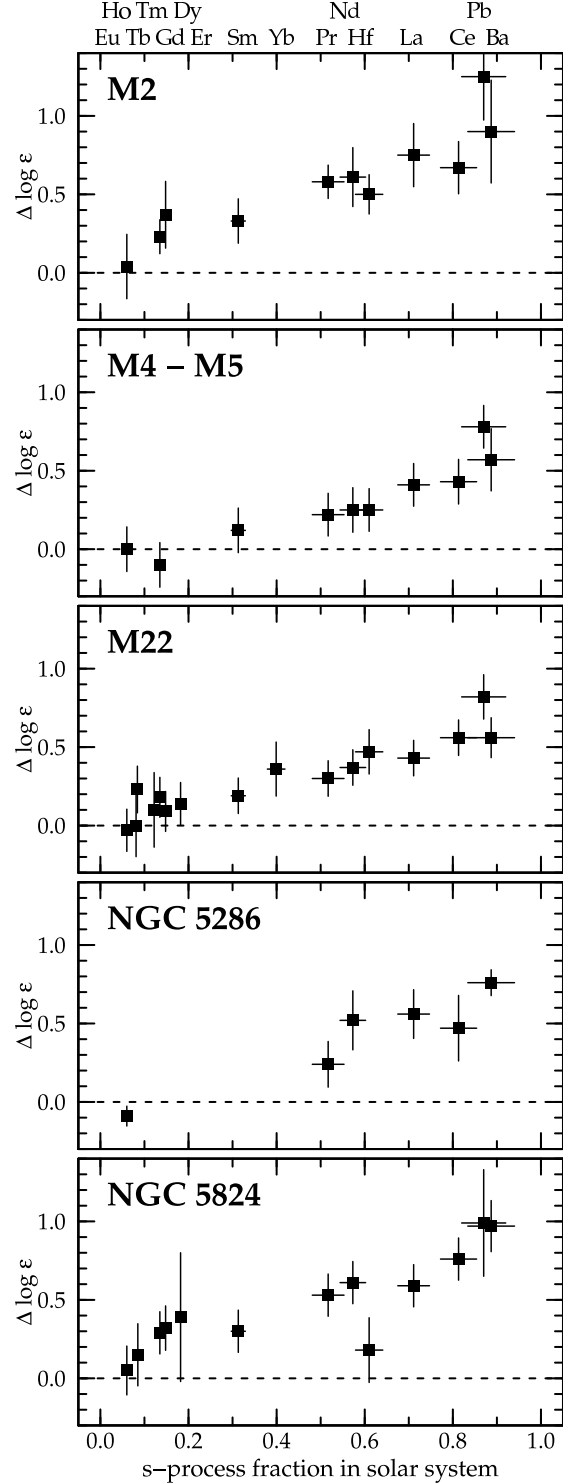


Figure 17. Abundance enhancement due to the s -process in globular clusters M2 (Yong et al. 2014b), M4 (Ivans et al. 1999, 2001; Yong et al. 2008a,b), M22 (Roederer et al. 2011), NGC 5286 (Marino et al. 2015), and NGC 5824. In M2, M22, NGC 5286, and NGC 5824, the abundance differences are computed in the sense of “ $r+s$ minus r -only.” In M4, the difference is computed in the sense of “M4 minus M5.” The s -process solar system fractions are taken from the models of Bisterzo et al. (2011). Only elements with $Z \geq 56$ are shown, since processes other than the r - and s -process may contribute to the lighter n -capture elements.

not C-enhanced before evolving up the RGB (Section 10.1). It is also not C-enhanced when evaluated by its C/O ratio, which is $\ll 1$, even if the LTE O abundance is overestimated by 1 dex. Both models and observations support this view. All of the low-metallicity models of Cristallo et al. (2015) end the TP-AGB phase with $C/O > 1$. The compilation of Masseron et al. (2010) lists 11 CEMP-*s* stars with $[Fe/H] > -3$, and all have $C/O > 1$.

The $[Ba/Fe]$, $[La/Fe]$, $[Ce/Fe]$, $[Pb/Fe]$, and other ratios in CEMP-*s* stars are usually several dex higher than the solar ratios and significantly higher than the ratios observed in star 61005163 in NGC 5824 (e.g., Van Eck et al. 2001; Sneden, Preston, & Cowan 2003; Aoki et al. 2008; Allen et al. 2012). The lack of radial velocity variations, lack of C enhancement, and relatively low $[n\text{-capture}/Fe]$ ratios collectively support our assertion that star 61005163 is not related to the stars in the CEMP-*s* class.

Searches for Ba-enhanced stars in normal globular clusters have found that the fraction of such stars (5 out of 1205, or 0.4 per cent; D’Orazi et al. 2010) is lower than in the field (> 8 per cent; Aoki et al. 2015). Only two such stars in clusters have been confirmed observationally from the analysis of many elements (Kacharov et al. 2013; Cordero et al. 2015). The n -capture abundance pattern in one of them, Lee 4710 in cluster 47 Tuc, is consistent with s -process enrichment from an AGB companion with an initial mass of $\sim 1.3 M_{\odot}$ (Cordero et al.) No such comparison was performed for the other star, in globular cluster M75. One simple explanation for the lack of Ba-enhanced stars could be the dense stellar environments of globular clusters, which would disrupt most wide binary systems and produce a lower binary fraction than in the field (cf., e.g., Côte et al. 1996; Mayor et al. 1996; Milone et al. 2012).

One star out of 26 (4 per cent) analyzed by us shows an anomalous abundance pattern. Finding additional stars with abundance patterns like star 61005163 in NGC 5824 would greatly alleviate the concerns that the composition of this particular star does not reflect its natal composition. At first glance, this percentage is much lower than the percentage of spectroscopically-confirmed members of the $r + s$ groups in other clusters: M2 (40 per cent, 10 stars total), M22 (40 per cent, 35 stars total), and NGC 5286 (43 per cent, 7 stars total). However, it is important to recognize that those samples are highly biased in favor of stars in the $r + s$ groups. More representative percentages can be estimated from photometric analyses of the multiple subgiant or red giant sequences (which correspond to the r -only and $r + s$ groups), for example. The populations associated with the $r + s$ groups in M2, M22, and NGC 5286 comprise only 3 per cent, 40 per cent, and 14 per cent of stars (Milone et al. 2015b; Piotto et al. 2012; Marino et al. 2015). NGC 5824 is not an outlier with respect to other complex clusters in this regard. It would be of great interest to obtain new ultraviolet broadband photometry of NGC 5824 with the *Hubble Space Telescope* (cf. Piotto et al. 2015) to search for the presence of multiple sequences in this cluster.

10.5 The Origin of the s -process Material

Stars in most low-metallicity globular clusters only show enrichment patterns like that found in the r -only group in NGC 5824. Three other low-metallicity clusters host groups

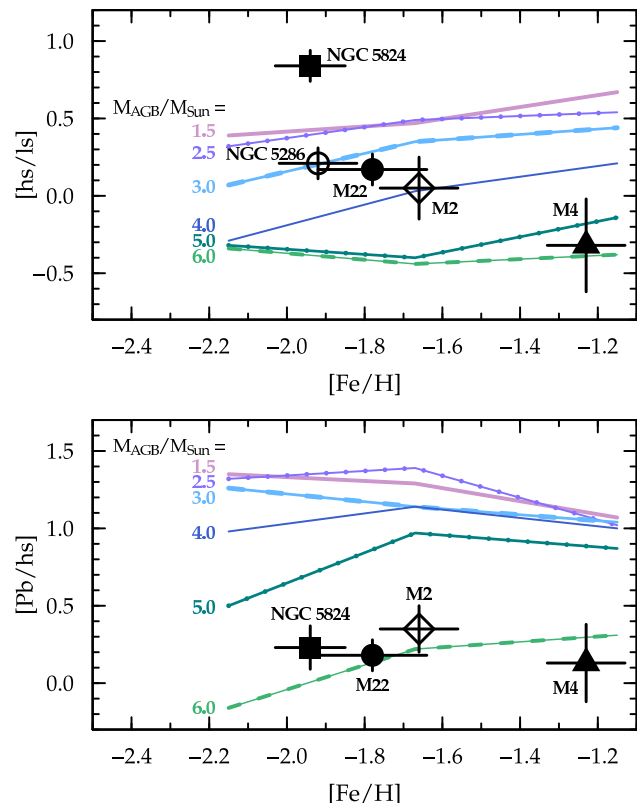


Figure 18. Comparison of the $[hs/ls]$ and $[Pb/hs]$ indices in five globular clusters and AGB model predictions from the FRUITY database (Cristallo et al. 2015). In M4, the s -process residual is computed using the abundance pattern in the (physically unrelated) globular cluster M5 as the r -only group. In NGC 5824, the difference is computed in the sense of “star 61005163 minus 42009955.” We recompute the $[hs/ls]$ and $[Pb/hs]$ indices using our definitions and the yields of the FRUITY database.

of stars resembling the distinct r -only and $r + s$ patterns: M2 (Yong et al. 2014b), M22 (Marino et al. 2009, 2011; Roediger et al. 2011), and NGC 5286 (Marino et al. 2015). All stars in another low-metallicity cluster, M4, resemble the $r + s$ pattern (Ivans et al. 1999; Yong et al. 2008a,b), thus distinguishing this cluster from other low-metallicity ones. In this section we examine the n -capture elements in M2, M4, M22, and NGC 5286, along with NGC 5824, to attempt to constrain the mass range of AGB stars that may have polluted the cluster ISM from which star 61005163 formed.

Figure 17 illustrates the differences between the $r + s$ and r -only groups in these five clusters. In all cases, $\Delta \log \epsilon$ is calculated as “ $r + s$ minus r -only” (or “ s -rich minus s -poor” in other nomenclature; e.g., Marino et al. 2011). We use the globular cluster M5, whose n -capture elements originated mainly in some form of r -process nucleosynthesis (Ivans et al. 2001; Yong et al. 2008a,b; Lai et al. 2011), as a foil for M4 to perform the subtraction “M4 minus M5.” Qualitatively, the abundance patterns in these five physically-unrelated clusters are remarkably similar, which could indicate that they share similar chemical enrichment histories.

We compute a few indices from well-measured abundance ratios to serve as indicators of the s -process nucleosynthesis patterns. We define $[ls/Fe] = ([Y/Fe] + [Zr/Fe])/2$,

$[hs/Fe] = ([La/Fe] + [Ce/Fe] + [Nd/Fe])/3$, $[hs/ls] = [hs/Fe] - [ls/Fe]$, and $[Pb/hs] = [Pb/Fe] - [hs/Fe]$. These definitions are constructed so that all ratios are measured in each of the five clusters, and thus they differ slightly from some versions of $[ls/Fe]$ and $[hs/Fe]$ in the literature. These indices are computed from the s -process residual in each cluster, not the derived ratios in the $r + s$ groups. The indices $[hs/ls]$ and $[Pb/hs]$, unlike $[X/Fe]$ ratios, are insensitive to the details of how material was acquired by the star observed today. For NGC 5824, $[hs/ls] = +0.84 \pm 0.10$, and $[Pb/hs] = +0.23 \pm 0.14$. Qualitatively speaking, the elements at the second s -process peak (Ba, La, Ce, Pr, Nd) are significantly overproduced relative to the elements at the first s -process peak (Sr, Y, Zr) and mildly underproduced relative to one of the elements at the third s -process peak (Pb).

The AGB models in the FRUITY database are computed at several metallicities that bracket the metallicities of the clusters of interest. The differing neutron fluxes, ambient physical conditions, and subsequent AGB evolution affect the s -process yields to produce a substantial dependence on the mass of the AGB progenitor. We overlay these predictions on the cluster values shown in Figure 18. A few points are notable. First, the $[hs/ls]$ index in NGC 5824 is higher by ≈ 0.6 dex than the next-highest cluster, although the $[hs/ls]$ indices in the other four clusters span a range of ≈ 0.5 dex. No single model from the FRUITY database can reproduce the $[hs/ls]$ index in NGC 5824, and the models would predict AGB masses ranging from ≈ 3 to $6 M_{\odot}$ for the other four clusters. Second, the $[Pb/hs]$ index in NGC 5824 is in very good agreement with the other three clusters where Pb has been detected. The models consistently imply AGB masses $\approx 6 M_{\odot}$ based on the $[Pb/hs]$ index. The models predict AGB masses of $\approx 6 M_{\odot}$ produced the s -process material in M4; however, for all other clusters, no single mass model can self-consistently account for the observed indices.

In principle, the timescale for star formation and chemical enrichment in each cluster matches the lifetime of the lowest-mass stars known to contribute to the metals in the present-day stars. A $6 M_{\odot}$ star has a lifetime of ≈ 60 Myr, while a $3 M_{\odot}$ star has a lifetime of ≈ 300 Myr. Roederer et al. (2011) examined tables of AGB nucleosynthesis yields and concluded that AGB stars with $M > 3 M_{\odot}$ were responsible for producing the s -process material in M22, implying a formation timescale of ≈ 300 Myr or less. Straniero, Cristallo, & Piersanti (2014) re-examined the M22 abundances derived by Roederer et al. using a self-consistent approach to the AGB models, integrating the yields of all stars above a certain mass and weighting by the initial mass function. They confirmed the suspicions of Roederer et al., deriving a timescale of 144 ± 49 Myr for M22, requiring the yields from AGB stars with masses $> 4 M_{\odot}$ or so. Shingles et al. (2014) adopted a different set of models and found a minimum enrichment timescale of $\approx 300 \pm 60$ Myr, with slightly lower-mass AGB stars contributing. The difference between the two results can be attributed to the prescription for the formation of the ^{13}C pocket in AGB stars with $3 < M/M_{\odot} < 4.5$. Both timescales are consistent with the maximum age spread allowed (~ 300 Myr) by the split subgiant branch in M22 (Marino et al. 2012).

The weak s -process, which operates in massive

($\sim 25 M_{\odot}$), rapidly-rotating, low-metallicity stars, is another proposed mechanism for producing s -process material in the early universe (e.g., The, El Eid, & Meyer 2000; Pignatari et al. 2008). These rapidly-evolving stars leave little time for the s -process to flow to the highest-mass nuclei. Using Figure 1 of Frischknecht, Hirschi, & Thielemann (2012), we estimate that $[hs/ls]$ can take a wide range of values, but $[Pb/hs] < -0.6$ in all of their models. The $[Pb/hs]$ index is slightly super-solar in the four clusters shown in Figure 18, so this is not a likely candidate for the s -process material found in these clusters.

Detailed comparisons with AGB models, like the work of Straniero et al. (2014) or Shingles et al. (2014), are beyond the scope of the present study. The similarity of the $[Pb/hs]$ ratios between NGC 5824 and M22 argues for a relatively short (few hundred Myr or less) enrichment timescale for NGC 5824. We have no reason to discount the measurements that form the $[hs/ls]$ index in NGC 5824, but its value is quite different from that found in the other four clusters and predicted using low-metallicity AGB models. We recommend the issue be revisited should more stars in the $r + s$ group in NGC 5824 be found.

10.6 The ^{232}Th Nuclear Chronometer in NGC 5824

We derive an upper limit from the non-detection of the Th II line at 4019.13 Å in the MIKE spectrum of star 42009955. The ^{232}Th isotope is radioactive, and it can only be produced by r -process nucleosynthesis. We calculate an age of the r -process material in NGC 5824 by comparing the current ratio of ^{232}Th and a stable element produced by the r -process (Eu) with their initial production ratio (Table 9, Roederer et al. 2009). The current ratio, $\log \epsilon(\text{Th}/\text{Eu}) < -0.34 \pm 0.08$, implies an age greater than 0.3 Gyr. This is not a useful age constraint.

Alternatively, if we assume a relatively old age for NGC 5824 (e.g., Carretta et al. 2010a), we can use the $\log \epsilon(\text{Th}/\text{Eu})$ ratio to exclude the presence of a rare, poorly-understood aspect of r -process nucleosynthesis, the so-called “actinide boost” (Hill et al. 2002; Schatz et al. 2002). This phenomenon is characterized by enhanced Th abundances, and it is found in a handful of low-metallicity field stars. If NGC 5824 is 13 Gyr old, the radioactive decay from Th produced in an actinide boost would yield a current ratio of $\log \epsilon(\text{Th}/\text{Eu}) -0.17 \pm 0.07$, which is significantly higher than our upper limit. Younger ages for NGC 5824 would imply even higher $\log \epsilon(\text{Th}/\text{Eu})$ ratios, in sharper tension with our observed limit.

Roederer & Thompson (2015) summarized the Th abundances or upper limits reported for stars in six clusters. To this list we add NGC 5824 (and M75, Kacharov et al. 2013, which was inadvertently omitted). None of these clusters, including NGC 5824, show evidence of an actinide boost, hinting that it may not occur or its signature is diluted beyond recognition in globular cluster environments. This observation may help in the hunt to identify or exclude candidate sites for the actinide boost phenomenon.

11 SUMMARY

We have examined the first sets of high-resolution spectroscopic observations obtained for the luminous, metal-poor globular cluster NGC 5824. Fifty stars have been observed using the M2FS spectrograph at Magellan, and 26 of them have S/N sufficient to perform a detailed abundance analysis of 20 species of 17 elements. Two stars were re-observed using the MIKE spectrograph to achieve broader wavelength coverage.

We derive $\langle [\text{Fe}/\text{H}] \rangle = -1.94 \pm 0.02$ (statistical) ± 0.10 (systematic). We exclude the presence of an intrinsic metallicity spread among these 26 stars at the 0.08 dex level. Previous work by Da Costa et al. (2014) did not detect a metallicity spread among these 26 stars, either, and only detected a possible spread among the fainter stars in their sample. Other elements in the Fe group show no significant star-to-star dispersion, and their ratios are well-matched to those in field stars with similar stellar parameters and metallicities.

The $[\text{Mg}/\text{Fe}]$ ratios in NGC 5824 have a large star-to-star dispersion, 0.28 dex, which is only found among some luminous, metal-poor clusters like ω Cen, M3, M13, M15, NGC 2419, NGC 2808, NGC 4833, and NGC 6752. Our limited data on O, Na, and Al do not permit us to examine the details of the light-element correlations and anti-correlations produced by p -capture reactions. However, these elements vary with each other, and Mg, in the usual manner in the two stars observed with MIKE.

The n -capture abundance patterns in 25 of the 26 stars observed with M2FS are effectively identical and consistent with r -process nucleosynthesis patterns found in field stars with similar stellar parameters and metallicities. One star shows a significant enhancement of s -process material, as well. We consider, and dismiss, the possibilities that this star self-enriched or obtained the s -process material from a companion that passed through the AGB phase of evolution. The s -process pattern resembles that found in groups of stars in the other low-metallicity clusters M2, M22, and NGC 5286. Mounting evidence suggests that intermediate-mass AGB stars ($\approx 3\text{--}6 M_{\odot}$) were responsible for producing the s -process material during the time of star formation in these clusters. The percentage of s -process-enhanced stars in NGC 5824 is within the range of that found in other clusters in this peculiar class.

We close by noting that several other low-metallicity clusters show evidence for internal dispersion among the n -capture elements. M2, M22, and NGC 5286 have been discussed extensively in Section 10.5. Heavy element dispersion in clusters ω Cen (Smith et al. 2000; D’Orazi et al. 2011), M15 (e.g., Sneden et al. 1997; Otsuki et al. 2006; Worley et al. 2013), and NGC 1851 (Yong & Grundahl 2008; Villanova, Geisler, & Piotto 2010; Carretta et al. 2011) has been confirmed by multiple investigators. Compelling evidence for variations in M19 has been presented recently by Johnson et al. (2015b). Other clusters with more subtle variations or less secure evidence include 47 Tuc (Cordero et al. 2015), M75 (Kacharov et al. 2013), M80 (Carretta et al. 2015), NGC 362 (Carretta et al. 2013a), NGC 4372 (San Roman et al. 2015), and NGC 5897 (Koch & McWilliam 2014). We have not included these clusters in the discussion here due to their enormous complex-

ity, small sample sizes, or small numbers of n -capture elements studied. Spectroscopic followup observations of the n -capture elements in these clusters would be greatly welcomed.

ACKNOWLEDGMENTS

I.U.R. thanks G. Da Costa for thoughtful, encouraging discussions throughout the course of this study; D. Kelson and E. Villanueva for their assistance installing and maintaining the CarPy MIKE reduction pipeline; A. Koch for checking the list of clusters with possible n -capture variations; E. Olszewski, I. Thompson, and M. Walker for helping to make M2FS a reality; and V. Placco for sharing insights on CEMP star binaries. We appreciate our referee’s thoughtful comments that have substantially improved this manuscript. This research has made use of NASA’s Astrophysics Data System Bibliographic Services, the arXiv preprint server operated by Cornell University, the SIMBAD and VizieR databases hosted by the Strasbourg Astronomical Data Center, the Atomic Spectra Database (Kramida et al. 2014) hosted by the National Institute of Standards and Technology, and the R suite of software (R Core Team 2014). IRAF is distributed by the National Optical Astronomy Observatories, which are operated by the Association of Universities for Research in Astronomy, Inc., under cooperative agreement with the National Science Foundation. M.M. and J.I.B. gratefully acknowledge support from the U.S. National Science Foundation to develop M2FS (AST-0923160).

REFERENCES

- Aldenius M., Lundberg H., Blackwell-Whitehead R. 2009, *A&A*, 502, 989
- Allen D. M., Ryan S. G., Rossi S., Beers T. C., Tsangarides S. A. 2012, *A&A*, 548, A34
- Alonso A., Arribas S., Martínez-Roger C. 1999, *A&AS*, 140, 261
- Aoki W., Beers T. C., Christlieb N., Norris J. E., Ryan S. G., Tsangarides S. 2007, *ApJ*, 655, 492
- Aoki W., et al. 2008, *ApJ*, 678, 1351
- Aoki W., Suda T., Beers T. C., Honda S. 2015, *AJ*, 149, 39
- Asplund M. 2005, *ARA&A*, 43, 481
- Asplund M., Grevesse N., Sauval A. J., Scott P. 2009, *ARA&A*, 47, 481
- Bailey III J. I., Mateo M. L., Bagish A., Crane J., Slater C. T. 2012, *Proc. SPIE*, 8446, 5G-1
- Bedell M., Meléndez J., Bean J. L., Ramírez I., Leite P., Asplund M. 2014, *ApJ*, 795, 23
- Beers T. C., Christlieb N. 2005, *ARA&A*, 43, 531
- Bellazzini M., et al. 2008, *AJ*, 136, 1147
- Bernstein R., Sheckman S. A., Gunnels S. M., Mochnacki S., Athey A. E. 2003, *Proc. SPIE*, 4841, 1694
- Bessell M. S. 1979, *PASP*, 91, 589
- Biémont É., Garnir H. P., Palmeri P., Li Z. S., Svanberg S. 2000, *MNRAS*, 312, 116
- Biémont É., et al. 2011, *MNRAS*, 414, 3350
- Bisterzo S., Gallino R., Straniero O., Cristallo S., Käppeler F. 2011, *MNRAS*, 418, 284

- Bohlin R. C., Hill J. K., Jenkins E. B., Savage B. D., Snow Jr., T. P., Spitzer Jr., L., York D. G. 1983, *ApJS*, 51, 277
- Booth A. J., Blackwell D. E., Petford A. D., Shallis M. J. 1984, *MNRAS*, 208, 147
- Brocato E., Buonanno R., Malakhova Y., Piersimoni A. M. 1996, *A&A*, 311, 778
- Carballo-Bello J. A., Sollima A., Martínez-Delgado D., Pila-Díez B., Leaman R., Fliri J., Muñoz R. R., Corral-Santana J. M. 2014, *MNRAS*, 445, 2971
- Cardelli J. A., Clayton G. C., Mathis J. S. 1989, *ApJ*, 345, 245
- Carretta E., 2014, *ApJL*, 795, L28
- Carretta E., Bragaglia A., Gratton R. G., Lucatello S., Momany Y. 2007, *A&A*, 464, 927
- Carretta E., et al. 2009a, *A&A*, 505, 117
- Carretta E., Bragaglia A., Gratton R., Lucatello S. 2009b, *A&A*, 505, 139
- Carretta E., Bragaglia A., Gratton R. G., Recio-Blanco A., Lucatello S., D'Orazi V., Cassisi S. 2010a, *A&A*, 516, A55
- Carretta E., et al. 2010b, *A&A*, 520, A95
- Carretta E., et al. 2010c, *ApJL*, 722, L1
- Carretta E., Lucatello S., Gratton R. G., Bragaglia A., D'Orazi V. 2011, *A&A*, 533, A69
- Carretta E., et al. 2013a, *A&A*, 557, A138
- Carretta E., Gratton R. G., Bragaglia A., D'Orazi V., Lucatello S., Sollima A., Sneden C. 2013b, *ApJ*, 769, 40
- Carretta E., et al. 2014, *A&A*, 564, A60
- Carretta E., et al. 2015, *A&A*, 578, A116
- Casagrande L., Ramírez I., Meléndez J., Bessell M., Asplund M. 2010, *A&A*, 512, A54
- Casagrande L., et al. 2014, *MNRAS*, 439, 2060
- Castelli F., Kurucz R. L. 2003, *Proc. IAU Symp. No 210, Modelling of Stellar Atmospheres*, N. Piskunov et al., eds., A20 (arXiv:0405087)
- Cohen J. G. 2011, *ApJL*, 740, L38
- Cohen J. G., Kirby E. N. 2012, *ApJ*, 760, 86
- Cohen J. G., Kirby E. N., Simon J. D., Geha M. 2010, *ApJ*, 725, 288
- Cordero M. J., Hansen C. J., Johnson C. I., Pilachowski C. A. 2015, *ApJL*, 808, L10
- Correnti M., Bellazzini M., Dalessandro E., Mucciarelli A., Monaco L., Catelan M. 2011, *MNRAS*, 417, 2411
- Côte P., Pryor C., McClure R. D., Fletcher J. M., Hesser J. E. 1996, *AJ*, 112, 574
- Cowan J. J., et al. 2002, *ApJ*, 572, 861
- Cowan J. J., et al. 2005, *ApJ*, 627, 238
- Cox A. N. 2000, *Allen's Astrophysical Quantities*, Springer-Verlag, New York, p. 340–341
- Cristallo S., Straniero O., Piersanti L., Gobrecht D. 2015, *ApJS*, in press (arXiv:1507.07338)
- Da Costa G. S., Held E. V., Saviane I., Guilleuszik M. 2009, *ApJ*, 705, 1481
- Da Costa G. S., Held E. V., Saviane I. 2014, *MNRAS*, 438, 3507
- Den Hartog E. A., Lawler J. E., Sneden C., Cowan J. J. 2003, *ApJS*, 148, 543
- Den Hartog E. A., Lawler J. E., Sneden C., Cowan J. J. 2006, *ApJS*, 167, 292
- Den Hartog E. A., Lawler J. E., Sobeck J. S., Sneden C., Cowan J. J. 2011, *ApJS*, 194, 35
- Di Criscienzo M., et al. 2011, *MNRAS*, 414, 3381
- D'Orazi V., Gratton R., Lucatello S., Carretta E., Bragaglia A., Marino A. F. 2010, *ApJL*, 719, L213
- D'Orazi V., Gratton R. G., Pancino E., Bragaglia A., Carretta E., Lucatello S., Sneden C. 2011, *A&A*, 534, A29
- Dubath P., Meylan G., Mayor M. 1997, *A&A*, 324, 505
- Fabbian D., Asplund M., Barklem P. S., Carlsson M., Kiselman D. 2009, *A&A*, 500, 1221
- Frebel A., Collet R., Eriksson K., Christlieb N., Aoki W. 2008, *ApJ*, 684, 588
- Frischknecht U., Hirschi R., Thielemann F.-K. 2012, *A&A*, 538, L2
- Gallino R., Arlandini C., Busso M., Lugaro M., Travaglio C., Straniero O., Chieffi A., Limongi M. 1998, *ApJ*, 497, 388
- Gonzalez G., Wallerstein G. 1998, *AJ*, 116, 765
- Gratton R. G., Sneden C., Carretta E., Bragaglia A. 2000, *A&A*, 354, 169
- Gratton R. G., et al. 2001, *A&A*, 369, 87
- Gratton R., Sneden C., Carretta E. 2004, *ARA&A*, 42, 385
- Gratton R. G., Carretta E., Bragaglia A., Lucatello S., D'Orazi V. 2010, *A&A*, 517, A81
- Grillmair C. J., Freeman K. C., Irwin M., Quinn P. J. 1995, *AJ*, 109, 2553
- Harris W. E. 1996, *AJ*, 112, 1487
- Hill V., et al. 2002, *A&A*, 387, 560
- Ibata R. A., Gilmore G., Irwin M. J. 1995, *MNRAS*, 277, 781
- IVANS I. I., Sneden C., Kraft R. P., Suntzeff N. B., Smith V. V., Langer G. E., Fulbright J. P. 1999, *AJ*, 118, 1273
- IVANS I. I., Kraft R. P., Sneden C., Smith G. H., Rich R. M., Shetrone M. 2001, *AJ*, 122, 1438
- IVANS I. I., Simmerer J., Sneden C., Lawler J. E., Cowan J. J., Gallino R., Bisterzo S. 2006, *ApJ*, 645, 613
- Ivarsson S., Litzén U., Wahlgren G. M. 2001, *Phys. Scr.*, 64, 455
- Johnson J. A., Bolte M. 2002, *ApJ*, 579, 616
- Johnson C. I., Pilachowski C. A. 2010, *ApJ*, 722, 1373
- Johnson C. I., Kraft R. P., Pilachowski C. A., Sneden C., IVANS I. I., Benman G. 2005, *PASP*, 117, 1308
- Johnson C. I., et al. 2015a, *AJ*, 149, 71
- Johnson C. I., Rich R. M., Pilachowski C. A., Caldwell N., Mateo M., Bailey III J. I., Crane J. D. 2015, *AJ*, 150, 63
- Kacharov N., Koch A., McWilliam A. 2013, *A&A*, 554, A81
- Kelson D. D. 2003, *PASP*, 115, 688
- King I. R., et al. 2012, *AJ*, 144, 5
- Koch A., McWilliam A. 2008, *AJ*, 135, 1551
- Koch A., McWilliam A. 2011, *AJ*, 142, 63
- Koch A., McWilliam A. 2014, *A&A*, 565, A23
- Kraft R. P., Sneden C., Smith G. H., Shetrone M. D., Langer G. E., Pilachowski C. A. 1997, *AJ*, 113, 279
- Kramida A., Ralchenko Y., Reader J., and the NIST ASD Team. 2014, *NIST Atomic Spectra Database (v. 5.2)*, online, URL: <http://physics.nist.gov/asd>
- Kunder A., et al. 2014, *A&A*, 572, A30
- Kurucz R. L., Bell B. 1995, Cambridge, MA: Smithsonian Astrophysical Observatory, CD-ROM 23
- Lai D. K., Smith G. H., Bolte M., Johnson J. A., Lucatello S., Kraft R. P., Sneden C. 2011, *AJ*, 141, 62
- Langer G. E., Fischer D., Sneden C., Bolte M. 1998, *AJ*, 115, 685
- Lawler J. E., Dakin J. T. 1989, *J. Opt. Soc. Am. B Optical Physics*, 6, 1457
- Lawler J. E., Bonvallet G., Sneden C. 2001, *ApJ*, 556, 452

- Lawler J. E., Wickliffe M. E., Cowley C. R., Sneden C. 2001a, *ApJS*, 137, 341
- Lawler J. E., Wickliffe M. E., Den Hartog E. A., Sneden C. 2001b, *ApJ*, 563, 1075
- Lawler J. E., Den Hartog E. A., Sneden C., Cowan J. J. 2006, *ApJS*, 162, 227
- Lawler J. E., Den Hartog E. A., Labby Z. E., Sneden C., Cowan J. J., Ivans I. I. 2007, *ApJS*, 169, 120
- Lawler J. E., Sneden C., Cowan J. J., Wyart J.-F., Ivans I. I., Sobeck J. S., Stockett M. H., Den Hartog E. A. 2008, *ApJS*, 178, 71
- Lawler J. E., Sneden C., Cowan J. J., Ivans I. I., Den Hartog E. A. 2009, *ApJS*, 182, 51
- Lawler J. E., Guzman A., Wood M. P., Sneden C., Cowan J. J. 2013, *ApJS*, 205, 11
- Lawler J. E., Wood M. P., Den Hartog E. A., Feigenson T., Sneden C., Cowan J. J. 2014, *ApJS*, 215, 20
- Li R., Chatelain R., Holt R. A., Rehse S. J., Rosner S. D., Scholl T. J. 2007, *Phys. Scr.*, 76, 577
- Lind K., Primas F., Charbonnel C., Grundahl F., Asplund M. 2009, *A&A*, 503, 545
- Lind K., Asplund M., Barklem P. S., Belyaev A. K. 2011, *A&A*, 528, A103
- Ljung G., Nilsson H., Asplund M., Johansson S. 2006, *A&A*, 456, 1181
- McLaughlin D. E., van der Marel R. P. 2005, *ApJS*, 161, 304
- McWilliam A. 1998, *AJ*, 115, 1640
- McWilliam A., Preston G. W., Sneden C., Searle L. 1995, *AJ*, 109, 2757
- Marino A. F., Milone A. P., Piotto G., Villanova S., Bedin L. R., Bellini A., Renzini A. 2009, *A&A*, 505, 1099
- Marino A. F., et al. 2011, *A&A*, 532, A8
- Marino A. F., et al. 2012, *A&A*, 541, A15
- Marino A. F., et al. 2014, *MNRAS*, 442, 3044
- Marino A. F., et al. 2015, *MNRAS*, 450, 815
- Mashonkina L., Ryabtsev A., Frebel A. 2012, *A&A*, 540, A98
- Massari D., et al. 2014, *ApJ*, 795, 22
- Masseron T., Johnson J. A., Plez B., Van Eck S., Primas F., Goriely S., Jorissen A. 2010, *A&A*, 509, A93
- Mateo M., Bailey III J. I., Crane J., Sheckman S., Thompson I., Roederer I., Bigelow B., Gunnels S. 2012, *Proc. SPIE*, 8446, 4Y-1
- Mayor M., Duquennoy A., Udry S., Andersen J., Nordstrom B. 1996, "The Origins, Evolutions, and Destinies of Binary Stars in Clusters," *ASP Conf. Ser. Vol. 90*, 190
- Mészáros S., et al. 2015, *AJ*, 149, 153
- Milone A. P. 2015, *MNRAS*, 446, 1672
- Milone A. P., et al. 2012, *A&A*, 540, A16
- Milone A. P., et al. 2013, *ApJ*, 767, 120
- Milone A. P., et al. 2015a, *ApJ*, 808, 51
- Milone A. P., et al. 2015b, *MNRAS*, 447, 927
- Mucciarelli A., Bellazzini M., Ibatá R., Merle T., Chapman S. C., Dalessandro E., Sollima A. 2012, *MNRAS*, 426, 2889
- Mucciarelli A., Bellazzini M., Merle T., Plez B., Dalessandro E., Ibatá R. 2015a, *ApJ*, 801, 68
- Mucciarelli A., Lapenna E., Massari D., Ferraro F. R., Lanzoni B. 2015b, *ApJ*, 801, 69
- Mucciarelli A., Lapenna E., Massari D., Pancino E., Stetson P. B., Ferraro F. R., Lanzoni B., Lardo C. 2015c, *ApJ*, in press (arXiv:150701596)
- Nave G., Johansson S., Learner R. C. M., Thorne A., Brault J. W. 1994, *ApJS*, 94, 221
- Navin C. A., Martell S. L., Zucker D. B. 2015, *MNRAS*, in press (arXiv:1507.04435)
- Nilsson H., Zhang Z. G., Lundberg H., Johansson S., Nordström, B. 2002, *A&A*, 382, 368
- Nilsson H., Ljung G., Lundberg H., Nielsen K. E. 2006, *A&A*, 445, 1165
- Norris J. E., Da Costa G. S. 1995, *ApJ*, 447, 680
- Olszewski E. W., Saha A., Knezek P., Subramaniam A., de Boer T., Seitzer P. 2009, *AJ*, 138, 1570
- Origlia L., et al. 2011, *ApJL*, 726, L20
- Origlia L., Massari D., Rich R. M., Mucciarelli A., Ferraro F. R., Dalessandro E., Lanzoni B. 2013, *ApJL*, 779, L5
- Otsuki K., Honda S., Aoki W., Kajino T., Mathews G. J. 2006, *ApJL*, 641, L117
- Pignatari M., Gallino R., Meynet G., Hirschi R., Herwig F., Wiescher M. 2008, *ApJL*, 687, L95
- Pilachowski C. A., Sneden C., Kraft R. P., Langer G. E. 1996, *AJ*, 112, 545
- Piotto G., et al. 2002, *A&A*, 391, 945
- Piotto G., et al. 2005, *ApJ*, 621, 777
- Piotto G., et al. 2007, *ApJL*, 661, L53
- Piotto G., et al. 2012, *ApJ*, 760, 39
- Piotto G., et al. 2015, *AJ*, 149, 91
- Placco V. M., Frebel A., Beers T. C., Stancliffe R. J. 2014, *ApJ*, 797, 21
- R Core Team, 2014, "R: A Language and Environment for Statistical Computing," R Foundation for Statistical Computing, Vienna, Austria. URL <http://www.R-project.org>
- Reed B. C., Hesser J. E., Shawl S. J. 1988, *PASP*, 100, 545
- Roederer I. U. 2011, *ApJL*, 732, L17
- Roederer I. U., Lawler J. E. 2012, *ApJ*, 750, 76
- Roederer I. U., Kirby E. N. 2014, *MNRAS*, 440, 2665
- Roederer I. U., Thompson I. B. 2015, *MNRAS*, 449, 3889
- Roederer I. U., Lawler J. E., Sneden C., Cowan J. J., Sobeck J. S., Pilachowski C. A. 2008, *ApJ*, 675, 723
- Roederer I. U., Kratz K.-L., Frebel A., Christlieb N., Pfeiffer B., Cowan J. J., Sneden C. 2009, *ApJ*, 698, 1963
- Roederer I. U., Sneden C., Lawler J. E., Cowan J. J. 2010a, *ApJL*, 714, L123
- Roederer I. U., Cowan J. J., Karakas A. I., Kratz K.-L., Lugaro M., Simmerer J., Farouqi K., Sneden C. 2010b, *ApJ*, 724, 975
- Roederer I. U., Marino A. F., Sneden C. 2011, *ApJ*, 742, 37
- Roederer I. U., et al. 2012a, *ApJL*, 747, L8
- Roederer I. U., et al. 2012b, *ApJS*, 203, 27
- Roederer I. U., Preston G. W., Thompson I. B., Sheckman S. A., Sneden C., Burley G. S., Kelson D. D. 2014a, *AJ*, 147, 136
- Roederer I. U., Cowan J. J., Preston G. W., Sheckman S. A., Sneden C., Thompson I. B. 2014b, *MNRAS*, 445, 2970
- Ruffoni M. P., Den Hartog E. A., Lawler J. E., Brewer N. R., Lind K., Nave G., Pickering J. C. 2014, *MNRAS*, 441, 3127
- Ryan S. G., Aoki W., Norris J. E., Beers T. C. 2005, *ApJ*, 635, 349
- San Roman I., et al. 2015, *A&A*, 579, A6
- Saviane I., Da Costa G. S., Held E. V., Sommariva V.,

- Gullieuszik M., Barbuy B., Ortolani S. 2012, *A&A*, 450, A27
- Sbordone L., Salaris M., Weiss A., Cassisi S. 2011, *A&A*, 534, A9
- Schatz H., Toenjes R., Pfeiffer B., Beers T. C., Cowan J. J., Hill V., Kratz K.-L. 2002, *ApJ*, 579, 626
- Shetrone M. D. 1996, *AJ*, 112, 1571
- Shimanskaya N. N., Mashonkina L. I., Sakhibullin N. A. 2000, *Astron. Rep.*, 44, 530
- Shingles L. J., Karakas A. I., Hirschi R., Fishlock C. K., Yong D., Da Costa G. S., Marino A. F. 2014, *ApJ*, 795, 34
- Simmerer J., Ivans I. I., Filler D., Francois P., Charbonnel C., Monier R., James G. 2013, *ApJL*, 764, L7
- Smith V. V., Lambert D. L., Nissen P. E. 1998, *ApJ*, 506, 405
- Smith V. V., Suntzeff N. B., Cunha K., Gallino R., Busso M., Lambert D. L., Straniero O. 2000, *AJ*, 119, 1239
- Snedden C. A. 1973, Ph.D. Thesis, Univ. of Texas at Austin
- Snedden C., Kraft R. P., Shetrone M. D., Smith G. H., Langer G. E., Prosser C. F. 1997, *AJ*, 114, 1964
- Snedden C., Pilachowski C. A., Kraft R. P. 2000, *AJ*, 120, 1351
- Snedden C., et al. 2003, *ApJ*, 591, 936
- Snedden C., Preston G. W., Cowan J. J. 2003, *ApJ*, 592, 504
- Snedden C., Kraft R. P., Guhathakurta P., Peterson R. C., Fulbright J. P. 2004, *AJ*, 127, 2162.
- Snedden C., Cowan J. J., Gallino R. 2008, *ARA&A*, 46, 241
- Snedden C., Lawler J. E., Cowan J. J., Ivans I. I., Den Hartog E. A. 2009, *ApJS*, 182, 80
- Sobeck J. S., Lawler J. E., Sneden C. 2007, *ApJ*, 667, 1267
- Sobeck J. S., et al. 2011, *AJ*, 141, 175
- Straniero O., Cristallo S., Piersanti L. 2014, *ApJ*, 785, 77
- Takeda Y., Zhao G., Chen Y.-Q., Qiu H.-M., Takada-Hidai M. 2002, *PASJ*, 54, 275
- The L.-S., El Eid M. F., Meyer B. S. 2000, *ApJ*, 533, 998
- Truran J. E., Cowan J. J., Pilachowski C. A., Sneden C. 2002, *PASP*, 114, 1293
- Van Eck S., Goriely S., Jorissen A., Plez B. 2001, *Nature*, 412, 793
- Ventura P., D'Antona F., Di Criscienzo M., Carini R., D'Ercole A., Vesperini E. 2012, *ApJL*, 761, L30
- Villanova S., Geisler D., Piotto G. 2010, *ApJL*, 722, L18
- Wickliffe M. E., Lawler J. E., Nave G. 2000, *J. Quant. Spectrosc. Rad. Trans.*, 66, 363
- Wood M. P., Lawler J. E., Sneden C., Cowan J. J. 2013, *ApJS*, 208, 27
- Wood M. P., Lawler J. E., Sneden C., Cowan J. J. 2014a, *ApJS*, 211, 20
- Wood M. P., Lawler J. E., Den Hartog E. A., Sneden C., Cowan J. J. 2014b, *ApJS*, 214, 18
- Worley C. C., Hill V., Sobeck J., Carretta E. 2013, *A&A*, 553, A47
- Yong D., Grundahl F. 2008, *ApJ*, 672, L29
- Yong D., Grundahl F., Lambert D. L., Nissen P. E., Shetrone M. D. 2003, *A&A*, 402, 985
- Yong D., Grundahl F., Nissen P. E., Jensen H. R., Lambert D. L. 2005, *A&A*, 438, 875
- Yong D., Lambert D. L., Paulson D. B., Carney B. W. 2008a, *ApJ*, 673, 854
- Yong D., Karakas A. I., Lambert D. L., Chieffi A., Limongi M. 2008b, *ApJ*, 689, 1031
- Yong D., et al. 2013, *MNRAS*, 434, 3542
- Yong D., et al. 2014a, *MNRAS*, 439, 2638
- Yong D., et al. 2014b, *MNRAS*, 441, 3396
- Zinn R. 1980, *ApJ*, 241, 602